TECHNIQUES FOR ACQUIRING SUBSURFACE DISPLACEMENTS IN VISCOELASTIC MATERIALS*

R. C. DeHart, Director
L. U. Rastrelli, Manager
J. D. Michie, Research Engineer

Department of Structural Research
Southwest Research Institute
San Antonio, Texas

ABSTRACT

Two techniques are presented for the measurement of internal deformations in members composed of a large mass of load-bearing, viscoelastic material. In Part A, an embedded particle, X-ray scintillation detector system is described which acquires displacement data from cylindrical models (less than 6-inch diameter). A brief description of the X-ray facility and its operation, specimen design and casting are presented. Typical data are shown for radial displacements of embedded particles in cylindrical models under uniaxial loading and internal pressurization.

In Part B, a device is described that measures strain (up to 50%) on viscoelastic materials such as the binder used in solid-propellant motors. The transducer's active element is a mercury base fluid column of 6-mil diameter and 0.5-inch length. Although the gage described is designed for surface mounting, the basic concept is applicable to a device that can be embedded within a material. Complete information is presented regarding the transducer construction, calibration and evaluation testing.

I. INTRODUCTION

Structures composed of a large mass of load-bearing mat ...al involve a unique set of structural design and analysis problems. Basically, the difficulties stem from the fact that the technology is dependent on information limited to experimental observations of <u>surface</u> phenomena. For structures employing relatively thin sections of a material whose phenomenological behavior is well defined, observations of surface displacements are quite adequate. The established stress and strain analysis for such structures need not consider the variations of displacements through the member's thickness. As the thickness of the member increases, the exact nature of the load-induced distortions between the two observable surfaces becomes more significant and less definitive. Moreover, for certain materials whose deformational behavior is predictable and relatively simple, and for certain quasi-static mechanical and thermal loading conditions, it is analytically expedient and valid to make assumptions regarding, say, the strain gradients through the thickness. On the other hand, for those materials which exhibit time and temperature dependent, nonlinear phenomenological properties, such assumptions become less reliable.

In addition to the questions of analysis and design for, say, structural deflections, there are also the problems of structural integrity. While it is true that many types of fracture failures begin on the surface, it is equally true that many such failures propagate <u>into</u> the member rather than along the same surface. Moreover, there are modes of failure (for example, large, permanent distortions) that are undoubtedly significantly influenced by stresses and strains within the member. These problems and the mere fact that it seems unreasonable to base an entire technology on observations of only a fragmentary portion of the entire mass would seem to justify the need for measuring subsurface deformations.

A simple and direct approach to acquire subsurface intelligence is to utilize small, embedded particles as reference points and to monitor their relative movements. If these particles are not signal-generating devices, then their motions must be observed and measured optically or, in the case of an opaque material, by penetrating radiation. The embedded devices must be capable of sustaining normal casting, forming and curing procedures. In their final embedded form, the devices should be of such size, geometry and construction as to allow the surrounding material to deform naturally. This embedded particle approach has been used in obtaining measurements of internal displacements in subscale models of solid propellant grains. Small particles are embedded in the grains during casting and located by recording the relative attenuation of scanning X-ray beams. The technique used in locating and tracking individual particles and retrieving measurements of displacement is described in Part A.

A second approach is to employ minature embedded transducers which respond to subsurface strain. The size and construction of these devices should be of such a nature as to at least minimize, and preferably avoid, the introduction of local strain field distortions. Conventional electrical resistance strain gages have proved unsuitable due to their relatively narrow range of measurement (less than 10% strain). Also their rigid construction (metallic foil and wire) would reinforce the supple binder material, and greatly inhibit and distort any displacements which might otherwise occur. The device described in Part B has been developed to extend the strain gage concept into the viscoelastic field.

The authors gratefully acknowledge their appreciation to Mr. John Crowley, Structural Mechanics Branch of the Office of Naval Research for his guidance and advice and to Messrs. E. Anderson and R. D. Williams for their contribution to the program.

PART A
EMBEDDED PARTICLE, X-RAY DETECTION SYSTEM

X-ray Facility. Ouantitative measurements of surface and subsurface displacements in viscoelastic materials are obtained electromechanically by observing the movements of embedded particles with a microfocus X-ray facility (Figs. 1 and 2). [1, 2]* The system translates analog intelligence into relative, particle displacement data in the form of graphs and numerical readout.

A narrow X-ray beam is formed by reducing the electron beam to a focal ellipse of 0.001 inch on a tungsten target anode. This target anode is oriented such that the X-rays propagate in the direction of and impinge on a scintillation detector equipped with a slit collimator designed to inhibit parasitic radiation and permit the examination of an 0.0075 square-inch area. The scintillation detector output is introduced to a linear-amplifier and pulse height analyzer; the amplified signal drives a relative count-rate meter. This signal, in turn, provides excitation for the numerical readout equipment. In the test field between the X-ray anode target and the scintillation detector, the model grains, reference grid system (used for calibration), and attenuation shims are positioned by the motorized indexing system (Fig. 3).

The X-ray emitter and the scintillation detector are fixed in position. A mechanical system indexes the test module vertically and horizontally relative to the reference X-ray beam; mechanically linked to indexing systems are potentiometers. An electrical output is obtained which is linearly related to displacements relative to the X-ray beam. In one facility configuration, the potentiometric signal is fed directly to the x-axis of the x-y recorder.

---

*Superscript denotes references.

3

A more precise, electronic digital readout system (consisting of shaft encoders, logic modules, and printer) automatically records numbers proportional to scanning distances between reference grid wires and embedded particles. Basically, this system samples analog intelligence (as provided by the horizontal or vertical indexing shaft encoder and the count-rate meter), converts this intelligence to digital pulses, and prints out digitalized relative displacement data. The logic system controls the (a) six-place decimal counter accumulator, (b) reversible digital counter to hold pulses from the shaft encoder, and (c) six-column decimal printer. This system utilizes the output signal from the X-ray count-rate meter to generate the control timing required to determine the effective center location of each embedded particle.

Controlled loading of the models is accomplished with a pneumatic system for subjecting the model to uniaxial loadings (Fig. 4) and/or internally pressurizing cored models (Fig. 5). The loading and indexing systems are integrated, thereby permitting models to be scanned while under load.

For a model presenting a varying thickness to the X-ray beam (e.g., a cylinder in a diametrical scan) the base line of the count-rate meter output varies inversely to the specimen thickness (Fig. 6). Although the particles' position are adequately defined, the shift in the base line complicates the digital readout data. One relatively simple method of controlling this shift in base line is to add attenuation shims in the test field (Fig. 7); however, this technique is not feasible for large radial deformations. Another method* is to immerse the specimen into a rectangularly shaped reservoir containing a liquid whose density matches that of the specimen; the liquid offers negligible resistance to the specimens deformational behavior while effecting a constant material thickness/density specimen to the X-ray beam.

The X-ray facility presently has an accelerating voltage to the X-ray tube of 80 kilovolts peak value. The penetrating potential of the system for filled and unfilled polyurethane is shown in Figure 8. Although the present facility is limited to filled urethane specimens less than 6-inch thickness, the embedded particle detection technique can be extended to larger grain models by providing a higher X-ray beam energy level.

Readout Data. The x-y recorder traces graphically portray the nature of the readout data. Figure 9 depicts a typical longitudinal trace for free-standing cylinder with two embedded particles positioned along the cylinder's longitudinal axis. Figure 10 contains longitudinal traces for a "no-load" condition and for the specimen subjected to a subsequent, uniaxial compressive load of 40 psi. Of interest is the "sag" in the load trace; the

---

*A third method is to introduce a second X-ray beam that scans the model in the immediate vicinity of the first beam but does not include the particles; the two beams are electronically subtracted, leaving a constant base line.

transverse (radial displacement) restraint offered by the bonded top and bottom load surfaces resulted in a barrelling effect.

The digital printout is in the form of a six-digit number. For the combination of a 0.1000 inch pitch positioning lead screw and a 1500 pulse encoder, each inch of scan is divided into 18,000 parts; thus, one count on the printout is equal to 5.55×10^{-5} inch. The printout initially indicates the center of a grid wire or particle from an arbitrary point (Fig. 11). The system begins counting when the reset switch is manually activated at a fixed point of reference; a printout is made indicating the number of counts from the reference point. When the system is operating in automatic reset, the counter returns to zero at each printout; thus, the new reference point becomes the center of the preceding particle and the printout number conveys the traversed distance.

The precision with which the facility can measure the relative position of embedded particles was acquired by the experimental error analyses and calibration procedure described in Reference 3. The maximum standard deviation of the x-y recorder is ±0.007 inch (including a chart reading error of ±0.001 inch); for the digital readout system, the maximum standard deviation for scanning in either the horizontal or vertical direction is ±0.0002 inch.

Model Grain Preparation. The development of the casting technique began with a study to determine the degree of local disturbance caused by inclusions. For example, it was apparent that residual deformations would surround each inclusion as the result of shrinkage during curing. The intensity and distribution of such residuals would be dependent on the particle's material, rigidity, size and geometry. The distance between particles was also considered. If the particles were positioned too close to one another, spheres of disturbed material surrounding each inclusion would merge and tend to further distort behavioral patterns. Finally, there was the question of whether or not the particles and accompanying residuals would distort the load-induced strain (displacement) patterns.

Use was made of the fact that the transparent, unfilled binder (when viewed with polarized light) exhibited fringe patterns which were directly related to the principal strains. Discs were prepared to study the effect of particle geometry (rectangular prisms, cylinders and spheres) and materials (lead, steel and glass, and hollow, urethane spheres), and voids of various sizes and shapes. The particles' integrated effect on the strain distribution was evaluated by subjecting the discs to diametral, compressive loads. The results of these photoelastic observations are presented by Bynum, et al.[4]. As expected, the spherical particles provided the optimum geometric configuration; a spacing of twice the particles' diameter was found to be more than adequate in isolating one particle from another. The presence of rigid, spherical particles caused only negligible effects on the load-induced

strains patterns; the effects (if any) of subsurface spherical and tubular voids were not discernable.

Relative X-ray attenuations afforded by various types of inclusions and voids were evaluated in resolution studies involving both filled and unfilled, layered and unlayered grains with variable penetration thicknesses. Typical resolution traces along the longitudinal axes of cylindrical specimens are shown in Figures 12 through 15.

Although continuous-cast models with a random array of inclusions were found to be of some use, it became apparent that retrieval of displacement data was appreciably enhanced if the embedded particles were prepositioned to coincide with the grain's reference axes. For cylindrical specimens, inclusions arranged in a rectangular pattern in one or more radial planes provided the most effective particle configuration (Fig. 16).

Continuous and segmental casting procedures were developed to provide for predetermined, particle positioning. In segmental casting, a templet was used to position particles on the partially cured, exposed (upper) surface of a previously cast section. By carefully controlling the casting, curing and particle placement sequence, it was possible to construct a layered cylinder with each layer containing radially positioned pellets. However, as a result of the differential curing, the interface between two adjacent sections exhibited negligible, but nevertheless photoelastically discernable, transverse reinforcing effects*.

A subsequent, more effective particle positioning technique is illustrated in Figure 17. The particles were suspended on a 0.006-inch diameter wire during casting and curing. Prior to removing the specimen from its mold, the suspension wire was withdrawn leaving a small, tubular void between the particles. In photoelastic examinations of diametrically loaded discs, it was found that the combined effect of the particle and suspension wire void introduced no perceptible change in the photoelastic fringe patterns.

Free-standing and case-bonded cylindrical specimens with circular and star-shaped cores (Figs. 18 and 19, respectively) were used in the study as subscale models of solid propellant grains. The specimens' diameter (3 inches for a case-bonded, solid propellant grain without a core) was limited by the penetration-resolution capabilities of the X-ray device; the load mechanism restricted the length to 8 inches.

---

*In early, cylindrical specimens, the interface radial reinforcement was quite pronounced. Under large, uniaxial compressive loads, the surface radial displacements at the interface were found to be considerably less than the adjacent uninhibited portions of the cylinder.

<u>Representative Data.</u> The objectives of the test program were threefold: (a) to demonstrate the X-ray scintillation detection system's feasibility, (b) to determine the scope, accuracy, and reliability of the integrated detection - data readout equipment and (c) to generate internal displacement data. The initial experimental studies were designed around three basic model configurations:

Model	Length	Diameter	Core
A	6"	3"	None
B	6"	3"	1.5" circular
C	6"	3"	Star shape

Time-dependent effects were minimized by subjecting each specimen to increment loads at low load rate at one-hour intervals and then acquiring displacement data. The data, therefore, represent particle movements at a finite time (one hour). Specimens consisting of the three model configurations (A, B, and C) were prepared with the embedded particles positioned along a selected radius.

In Figure 20, radial* displacement is plotted against uniaxial stress, both true and apparent.** The deviation of the curves from linearity is not particularly significant as the specimen material (polyurethane) exhibits a nonlinear stress-strain relationship. In Figure 21, the same radial displacement data as shown in Figure 20 is plotted against initial particle position. Here the small deviation from linearity may be significant as each individual curve is less dependent on the material's stress-strain relationship.

In Figure 22, the radial displacement data for Model B under uniaxial load are shown. The curves for the lower uniformly distributed loads (5, 10 and 20 psi) appear linear; however, the 30 psi axially induced stress curve is nonlinear. The data for Model B under internal pressurization are shown in Figure 22 and appear to represent a linear relationship. An undetermined uniaxial load was applied to Model B during internal pressurization to provide the necessary pressure seal on the core; this load directly affects radial particle displacements and is, thus, undesirable. However, a miniature load cell is being introduced into the mechanical loading system which will measure and enable the control of this uniaxial force.

---

*The initial experiments were limited to radial displacement observations in lieu of longitudinal measurements as the radial data were considered to be of more immediate interest.

**Apparent stress is defined as the uniaxial load divided by a constant area (i.e., sectional area at no load); true stress is defined as the uniaxial load divided by the deformed area.

Model C, (star core) was cast in two configurations with the embedded particles arrayed across both the thick and thin wall sections. The comparison of Figures 24 and 25 indicate that the displacements vary with initial radial position (u_0), stress (σ) and wall thickness.

Summary. An X-ray scintillation-detector, coupled with data readout equipment and specimen positioning components, provides capabilities for measuring subsurface displacements with an acceptable (±0.0002 inch) degree of precision. Subscale propellant grains, when subjected to uniaxial loading and internal pressurization, exhibit relative discernable motions of embedded particles. By utilizing birefringent techniques, the degree of local disturbance caused by the inclusions, geometry, size and material can be predetermined. Small lead particles (1/16 inch diameter) spaced at least two particle diameters apart produce negligible effects on the load-induced strain patterns and provide the desired degree of X-ray beam attenuation. Several specimen casting techniques are available which enables the placement of the embedded particles in selected patterns.

Radial displacements obtained thus far indicate a deviation from linearity, particularly with increased load. Although the data presented are of a preliminary nature and limited in scope, indications are that the embedded particle technique is applicable to other model geometries, and loads, and those types of studies concerned with time and temperature dependent behavior of viscoelastic materials.

PART B
ELASTOMERIC STRAIN TRANSDUCER

Background. Conventional methods for measuring surface strains on elastic, metallic materials have proved ineffective when applied to the high elongations prevalent in viscoelastic bodies. This can be attributed to two basic limitations: (a) present strain measuring devices (such as wire or foil electrical resistance gages) have a relatively low useful strain range (less than 10%); and (b) reinforcing effects of a relatively rigid gage, when mounted on a viscoelastic material, distorts the strain field under investigation.

Several new concepts for measuring strains of large magnitude within a material were formulated, and the most promising concept was selected for further study. In order to demonstrate feasibility, a conceptual gage was designed and fabricated. The initial configuration consisted of a small, thick-wall elastomeric tube filled with an electrical conducting fluid. As expected, the electrical resistance of the fluid column changed as the elastomeric tube was axially deformed; this change in gage resistance was determined to be proportional (and nearly linear) to extensional deformations. Also, the prototype exhibited clearly discernible and measurable phenomena for elongations up to forty percent of its original length.

Three exploratory models are pictured in Figure 26: a triaxial module consisting of three orthogonal nonintersecting gages, a rosette containing three coplanar (nonintersecting) gages and a uniaxial module with a single active column.* Typical results of module testing are indicated in Figures 27 and 28. In Figure 27, a linear relationship between strain and resistance change is depicted for the uniaxial module in tension. In Figure 28, a similar relationship is shown for the triaxial module (Fig. 26) in compression; gages 2 and 3 reflect the module's two lateral expansions.

Further efforts were devoted to exploring the concept's potential and developing a practical, high-elongation strain transducer suitable of surface mounting. A general review of the progress which has been made is presented in the following discussion.

Gage Design and Fabrication. A preliminary gage configuration (Fig. 29) was selected to serve as a standard of comparison for the evaluation testing.[5] Although the elastomeric strain transducer concept is adaptable for both surface mounting and embedment, in the initial development studies the former mode was chosen because of (a) the ease with which the gages could be attached and removed from test articles used in the intermittent elongation-calibration procedures and (b) the gages' accessibility for comparative studies with optical and mechanical devices. A nominal gage length of 0.5 inch** was used for the initial prototype.

The initial elastomeric strain transducers were fabricated in three primary steps. The transducer body containing the gage length and conducting fluid reservoirs was cast from Adiprine L-100***. Reservoirs were formed by 15 mil outside diameter hypodermic needles and the gage length by a 6 mil steel wire‡. As shown in Figure 30, the steel wire was inserted through the hypodermic needles and held taut during the polyurethane casting and curing stages. The needles and wire were removed and the cured gage body was stripped from the mold; all surfaces which came in contact with the uncured polyurethane were coated with a teflon, mold release agent prior to casting. A mercury base alloy was injected into the reservoirs and gage length cavity with the necessary precautions to prevent entrapping of air or foreign particles. A two-wire terminal was inserted a precise distance into each reservoir to establish a low resistance wire-to-conductive fluid contact

---

*Aluminum channel at ends of uniaxial gage were bonded to the module to facilitate gripping during testing.

**Fabrication feasibility studies indicate that the gage length can be varied from 1/4 to 4 inches without a major modification to the basic design concept.

***Polyurethane compound by DuPont.

‡Gages have been fabricated employing a 3 mil and a 1 mil gage wire.

and to insure a consistent, nominal electrical resistance across the gage length. The gage body-lead wires composite was clamped into a mold fixture (Fig. 31a) which restrained any relative motion within the composite. A second casting of polyurethane provided the seal for the conductive fluid and anchored the leads to the gage body (Fig. 31b). The completed gage was a sturdy device capable of sustaining normal laboratory handling without damage.

An important aspect of the elastomeric transducer concept is the readout equipment and circuitry required to detect and measure resistance change in the gage. The strain transducer's relative low resistance (0.40 ohms for the 0.5 inch gage length) is particularly applicable to a Kelvin bridge circuit. Because of the Kelvin bridge circuit requirement, the elastomeric strain transducer configuration has the 2-two wire connection detail. Nevertheless, the gage configuration is applicable (without modification) to a Wheatstone bridge circuit.

Calibration Procedure. Establishment of elongation-resistance change relationship for each prototype gage was performed with the aid of a micrometer dial extensometer (Fig. 32). The gages were elongated in precise incremental distances and the electrical resistance across the strain transducer noted (Fig. 33).

In positioning a gage in the extensometer, it was determined the clamping force affected the electrical resistance. To eliminate this factor, the gage's configuration was modified to include four calibration lugs (Fig. 34). Subsequent tests performed on the modified gage indicated that the adverse effect of the extensometer clamping action had been eliminated. The original and modified strain transducer prototypes are shown in Figure 35; the calibration lugs can be removed after the gage is calibrated.

Preliminary Evaluations. In order to establish the elastomeric strain transducer's performance capability, a series of evaluation tests were devised and the prototype gages appraised according to their response.

Nominal Resistance. The nominal (nonstrained) electrical resistance within the first prototype gage group (the gages were manufactured in groups of six) was found to vary from 0.30 to 1.10 ohms. The desirability of fabricating gages with uniform mechanical properties was deemed of utmost importance as a standard gage would provide a higher degree of confidence and would greatly simplify the readout equipment and circuitry.

The initial gage group was examined radiographically. The examination clearly indicated the nominal resistance variations could be attributed to two basic factors: (a) the lead wire penetration distance differed from gage to gage and (b) the gage capillary contained air bubbles

within the mercury base alloy which were detectable only by radiographic examination. As mercury is more resistive than copper by a factor of 55, a small error in the distance between the copper wire leads (across the gage length) would result in a disproportionately large change in nominal electrical resistance. Similarly, the presence of foreign (dielectric) particles and air bubbles severely reduces the effective cross-sectional area of the capillary and thus alters the strain transducer's nominal resistance.

Both of these deficiencies were corrected by improved fabrication techniques. As illustrated in Figure 36, the nominal resistance range of 27 gages was 0.32 ohm (0.57 - 0.25); however, 85 per cent of the gages were within a 0.16-ohm range. Additional refinements in the design and fabrication of the strain transducer would undoubtedly yield a more uniform gage.

Elongation. Each gage was clamped in the extensometer and elongated to insure the gage's function over the expected strain range and to establish the relationship between resistance change and gage elongation. All gages demonstrated a need for several "shakedown" cycles in order to stabilize elongation-resistance change. These cycles were performed with the gage never remaining in the extended configuration in excess of one minute to minimize the plastic deformation of the gage body. However, the polyurethane gage body exhibits a near total creep recovery when deformed for long time intervals and then released. A typical elongation-resistance change curve is shown in Figure 33. The relationship is nearly linear over the 50 per cent strain range with a slight divergence from a constant slope within the initial 5 per cent strain and the 45 to 50 per cent strain segments. The slopes of 14 transducers' calibration curves are compared in the frequency distribution graph (Fig. 37); the values vary from 0.70 to 1.10 ohms per inch of elongation. The slopes of the calibration curves appear to be independent of the gages' nominal resistance.

Temperature Environment. To ascertain the effects of temperature on the transducer, three gages were subjected to four cycles of elevated temperatures; the results of these tests are indicated by the plot of a typical gage in Figure 38. The gage was heat-soaked at each temperature for a period of 30 minutes to insure a stable reading. A maximum test temperature of 285°F was selected to correspond to the curing temperature of the transducer's body. As indicated, there was an increase in gage resistance with an increase in temperature. This can be attributed to an accumulative effect of (a) change in capillary geometry due to the coefficient of thermal expansion and (b) change due to the coefficient of thermal resistivity. In general, the thermal effect appears to be reversible; however, the scatter of the data points would seem to indicate a lack of control of one or more experimental parameters during the gage evaluation. The possibility exists that the gages may require a "thermal shakedown" of 20 or 30 cycles before stabilizing into a predictable (and repeatable) thermal performance.

Pneumatic Environments. A potential application for the strain transducer would be on surfaces of materials immersed in a pressure environment. Accordingly, one of the preliminary tests consisted of subjecting three unmounted gages to a pressure environment. In Figure 39, the response characteristics of a typical gage is shown. There was a reduction of gage resistance with an increased pressure environment. Although the pneumatic environment tests were not conclusive, it was determined that pressurization duration was a critical factor as the gage body relaxed under the applied loading. Readings were taken at each load increment until the gage resistance stabilized. The data points shown in Figure 39 are terminal values measured after the pressure increment had been applied for a period of approximately ten minutes.

Summary. An elastomeric strain transducer has been developed which has the performance capabilities of retrieving displacement intelligence from viscoelastic materials and has a repeatable strain range of approximately 50 per cent. Performance studies of twenty-seven prototype gages, constructed and evaluated according to stability, repeatability, and thermal and pressure environmental effects, indicated promising capabilities and provided a basis for the development of an improved design.

In its present state of development, the strain transducer has application in both propellant grain and high performance tire studies. Nevertheless, future efforts will be devoted to refining the gage design by miniaturization and by increasing nominal gage resistance.

CONCLUSIONS

Two methods (the embedded particle, X-ray scintillation-detection facility and the elastomeric strain transducer) have been developed to explore surface and subsurface deformations in members composed of a large mass of viscoelastic material. The methods are independent in their operation but complementary in application. A qualitative comparison of the methods shows the following:

Characteristic	Embedded Particle	Strain Transducer
1. Readout Precision	Excellent	Fair
2. Continuous Readout	No	Yes
3. Readout Speed	Fair	Excellent
4. System Reliability	Good	Fair
5. Miniaturization	Good	Fair
6. Application		
a. Laboratory	Excellent	Good
b. Field	Fair	Good

Although their state of development is sufficiently advanced to acquire significant and meaningful data, each system is susceptible to being continually upgraded in its performance characteristics.

REFERENCES

1. Rastrelli, L. U., and DeHart, R. C., "Studies of Displacements in Solid Propellant Grains (Embedded Particle, X-Ray Detection System)," Interim Report, Project 03-1043, Contract No. NOnr-3363-(FBM), Sept. 1, 1962, Structural Mechanics Branch, Office of Naval Research, Washington 25, D. C.

2. Rastrelli, L. U., DeHart, R. C., and Michie, J. D., "Studies of Internal Displacements in Solid Propellant Grains (Embedded Particle, X-Ray Detection System," Interim Report, Project 03-1043, Contract No. NOnr-3363(00)(FBM), October 28, 1963, Structural Mechanics Branch, Office of Naval Research, Washington 25, D. C.

3. Rastrelli, L. U., and Pape, B. J., "Studies of Displacements in Solid Propellant Grains (Estimating Experimental Errors in X-Ray Detection Facility)," Interim Report, Project 03-1043, Contract No. NOnr-3363(00)(FBM), Sept. 5, 1962, Structural Mechanics Branch, Office of Naval Research, Washington 25, D. C.

4. Bynum, D. J., and Rastrelli, L. U., "Studies of Displacements in Solid Propellant Grains (Photoelastic Observations Using Tolylene Di-Isocyanote Polyurethane)," Interim Report, Project 03-1043, Contract No. NOnr-3363(00)(FBM), Aug. 20, 1962, Structural Mechanics Branch, Office of Naval Research, Washington 25, D. C.

5. Michie, J. D., Rastrelli, L. U., and DeHart, R. C., "Studies of Internal Displacements in Solid Propellant Grains (Elastomeric Strain Transducer)," Interim Report, Project 03-1043, Contract No. NOnr-3363(00)(FBM), March 20, 1965, Structural Mechanics Branch, Office of Naval Research, Washington 25, D. C.

C-21236
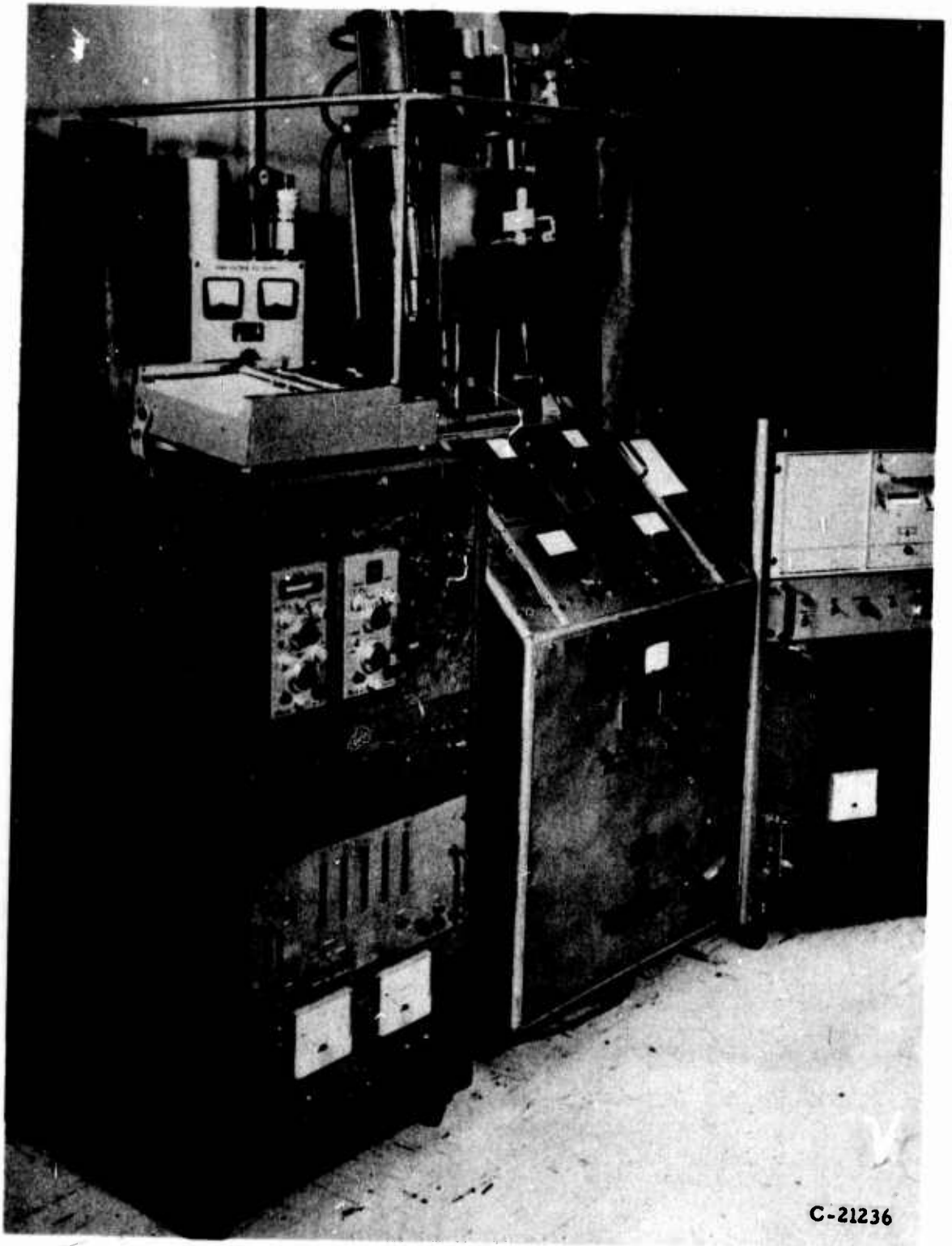
FIGURE 1   EMBEDDED PARTICLE, MICRO-FOCUS
X-RAY FACILITY

14
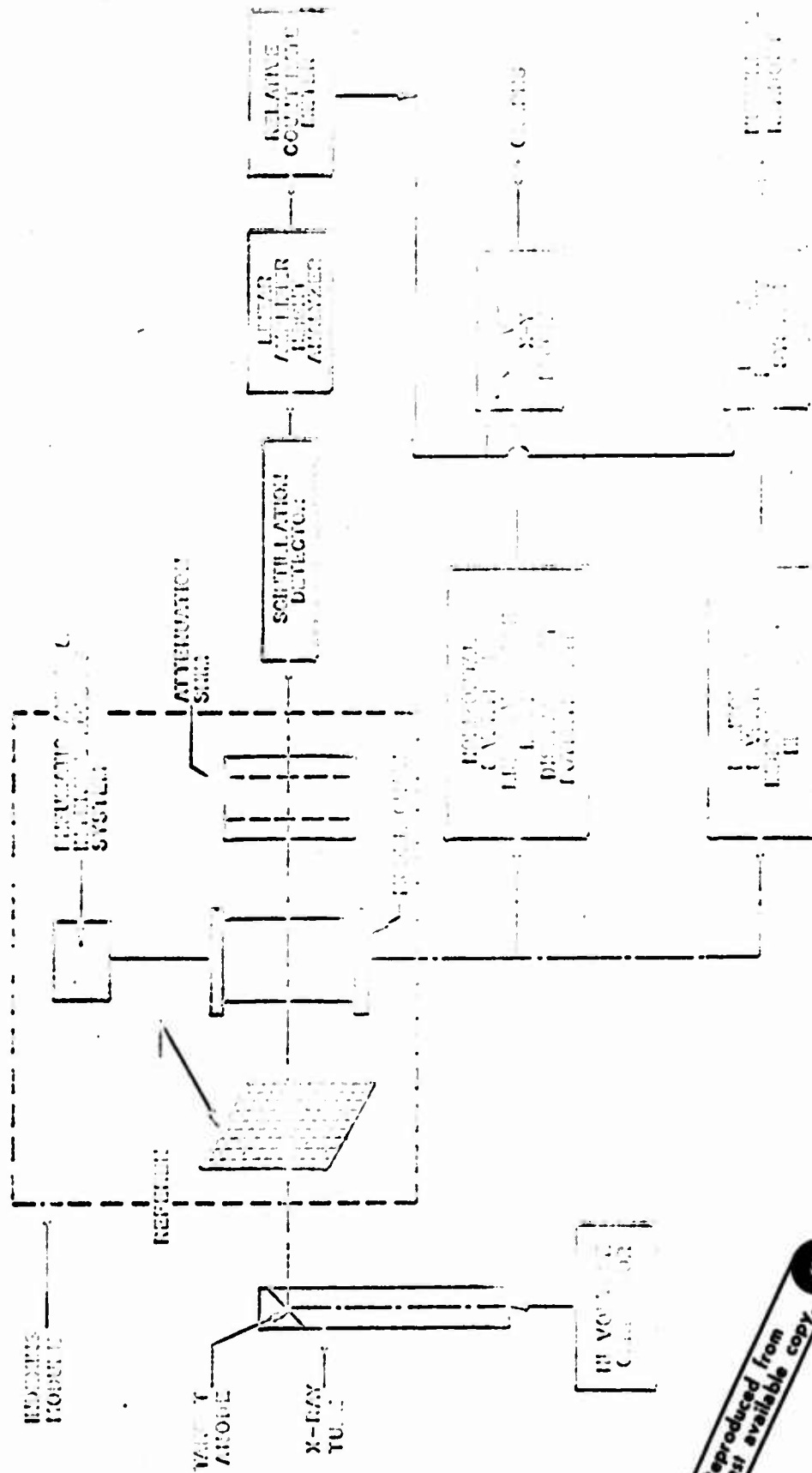
FIGURE 2   EMBEDDED PARTICLE, X-RAY DETECTION
FACILITY SCHEMATIC

15

PNEUMATIC LOAD MECHANISM

EXTERNAL REFERENCE GRID SYSTEM

MODEL GEAR

SCINTILLATION DETECTOR

ROTATIONAL

VERTICAL INDEX

HORIZONTAL INDEXING

X-RAY EMITTER
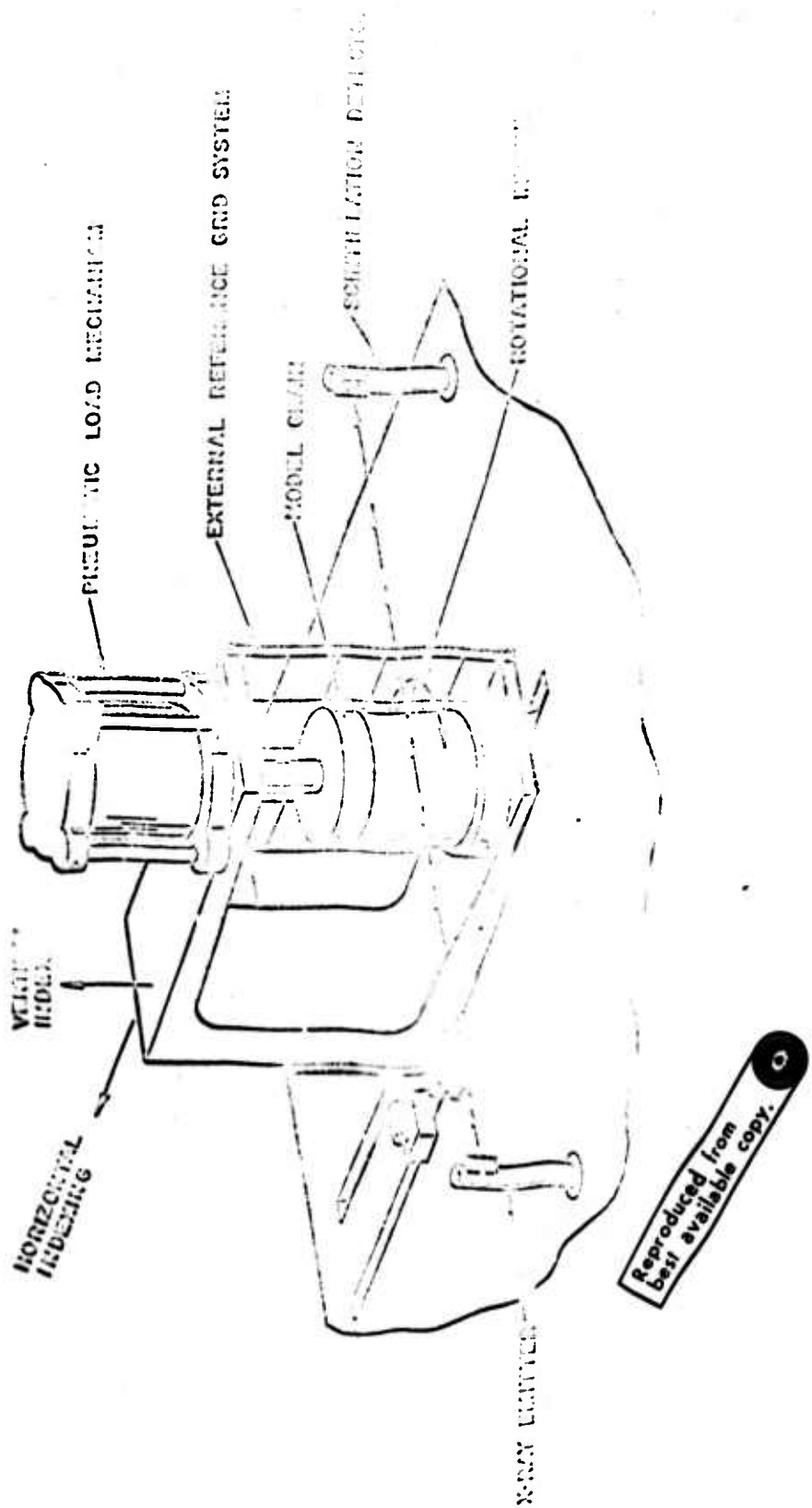
FIGURE 3 TEST MODULE INDEXING SYSTEM

16
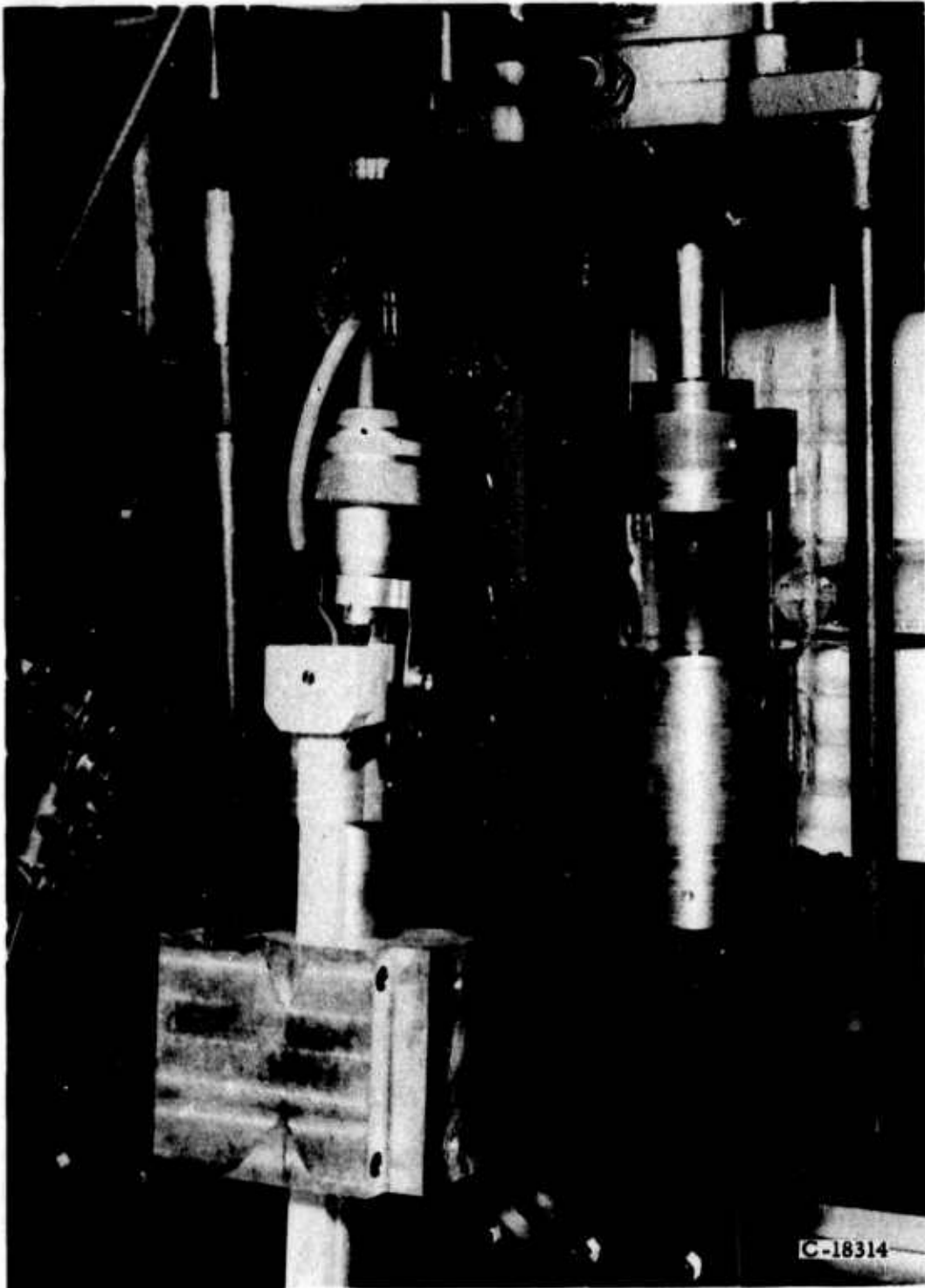
FIGURE 4   LOAD FIXTURE FOR UNIAXIAL
COMPRESSION OR TENSION

17

C-21237
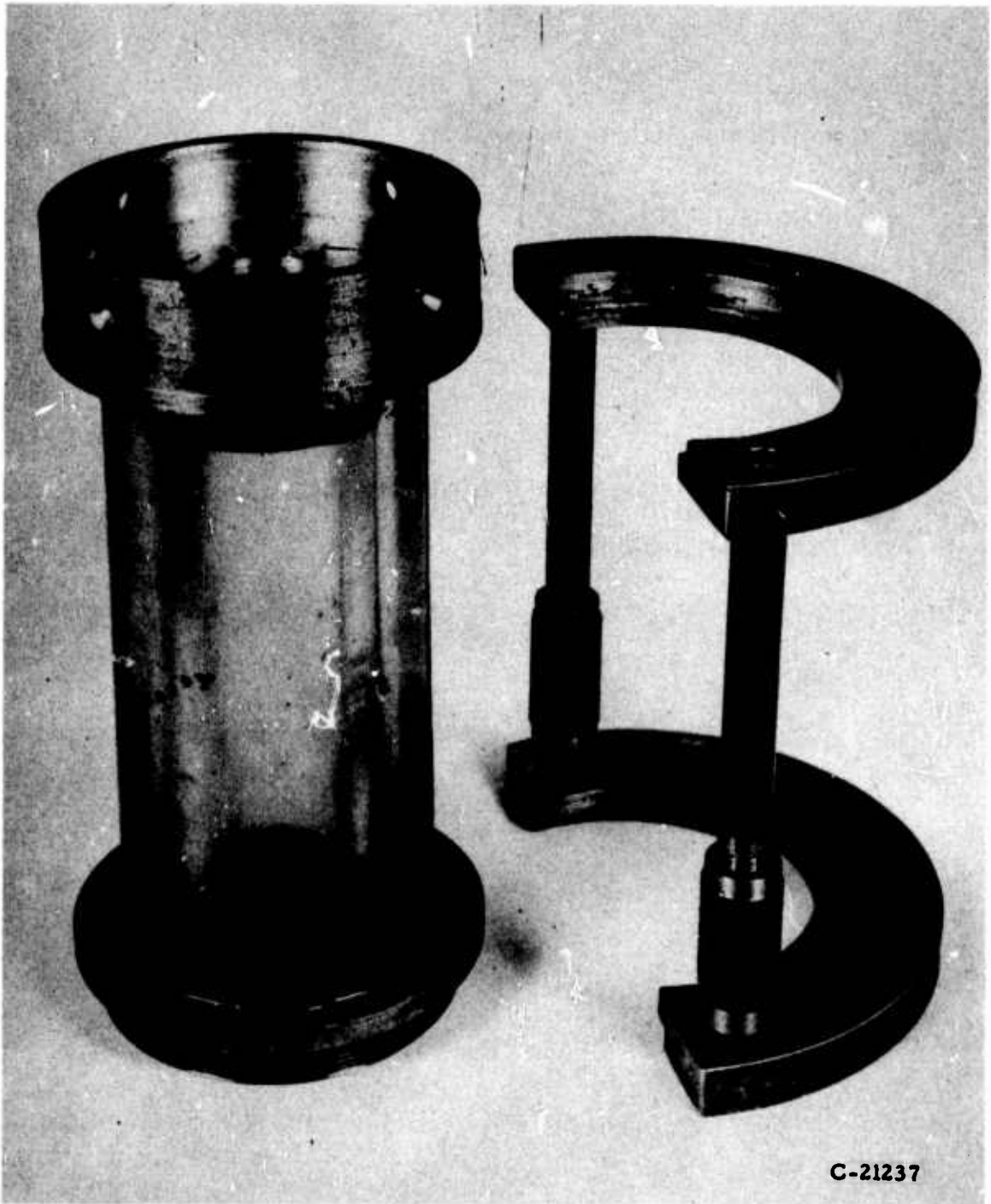
FIGURE 5   UNFILLED GRAIN BONDED TO ADAPTER PLATES
(CLAMP ON RIGHT PREVENTS SHORTING OF SPECIMEN
DURING INTERNAL PRESSURIZATION)

18
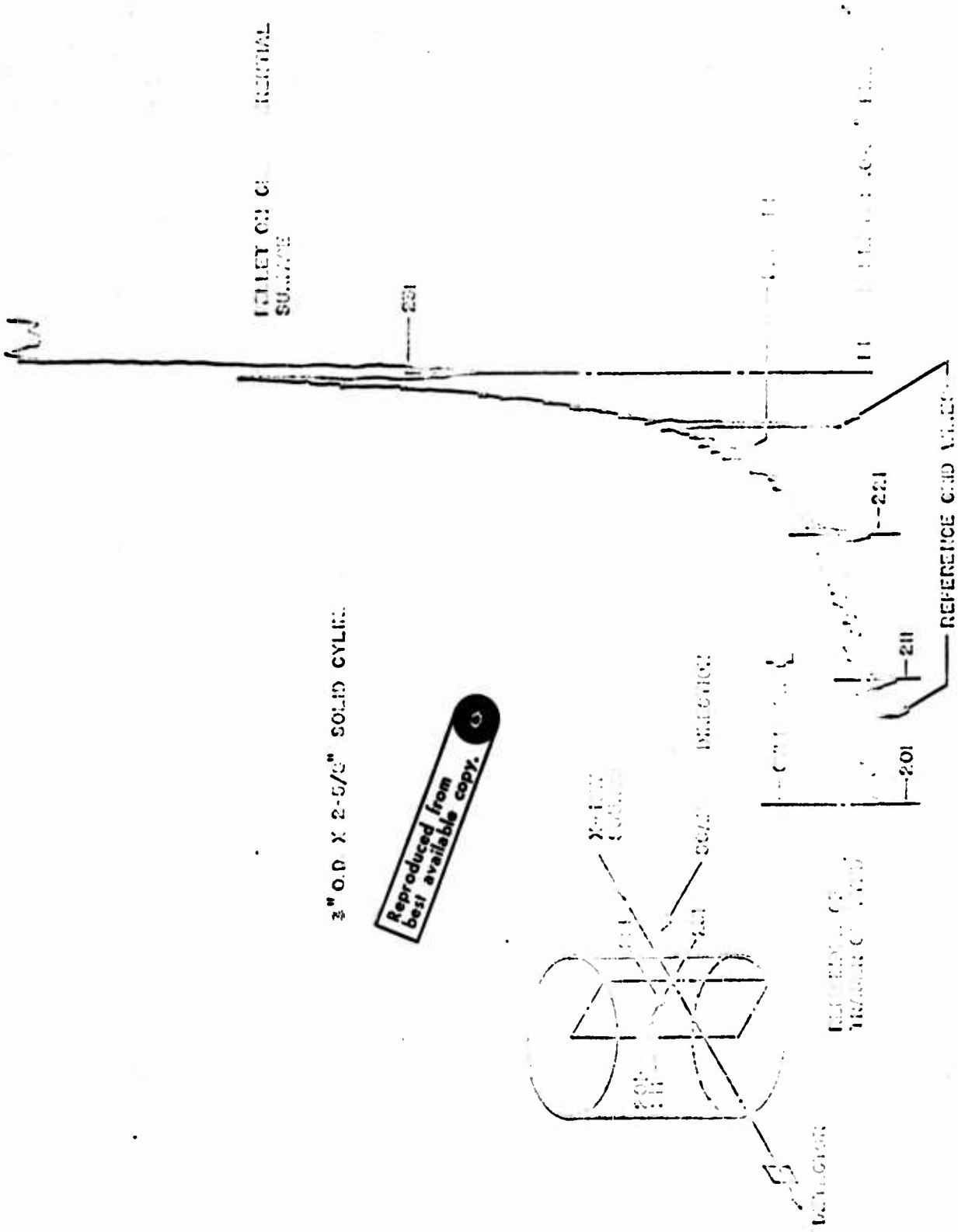
FIGURE 6   TYPICAL TRANSVERSE TRACE OF
FREE STANDING CYLINDER
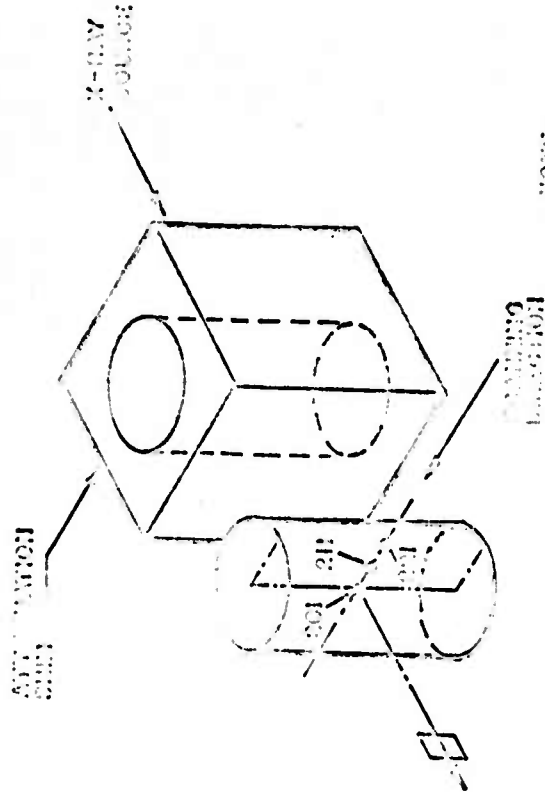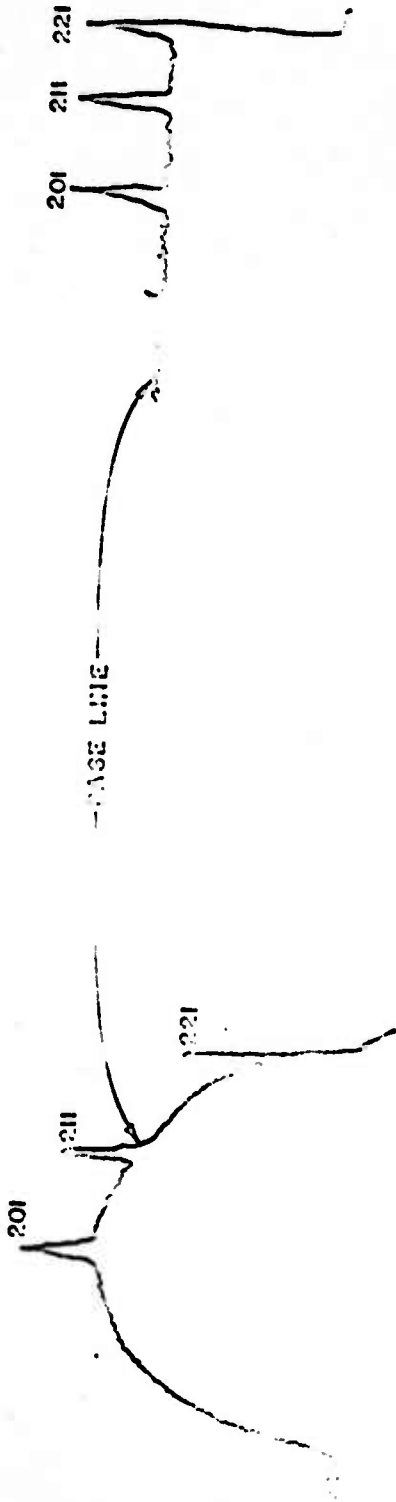
19
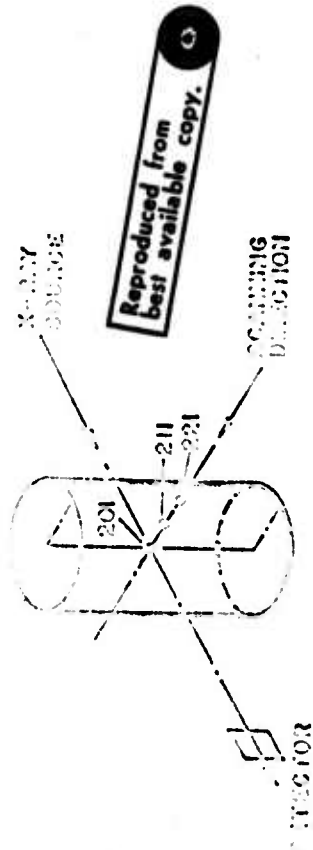
FIGURE 7 BASE LINE ADJUSTMENT BY USE OF
ATTENUATION SHIM(S)
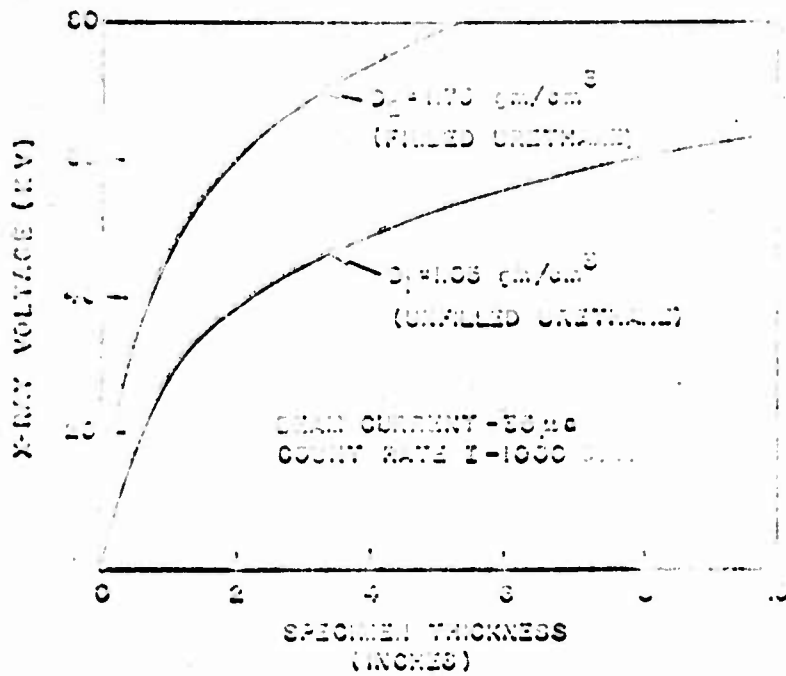
FIGURE 8   PENETRATING POTENTIAL OF X-RAY FACILITY

21
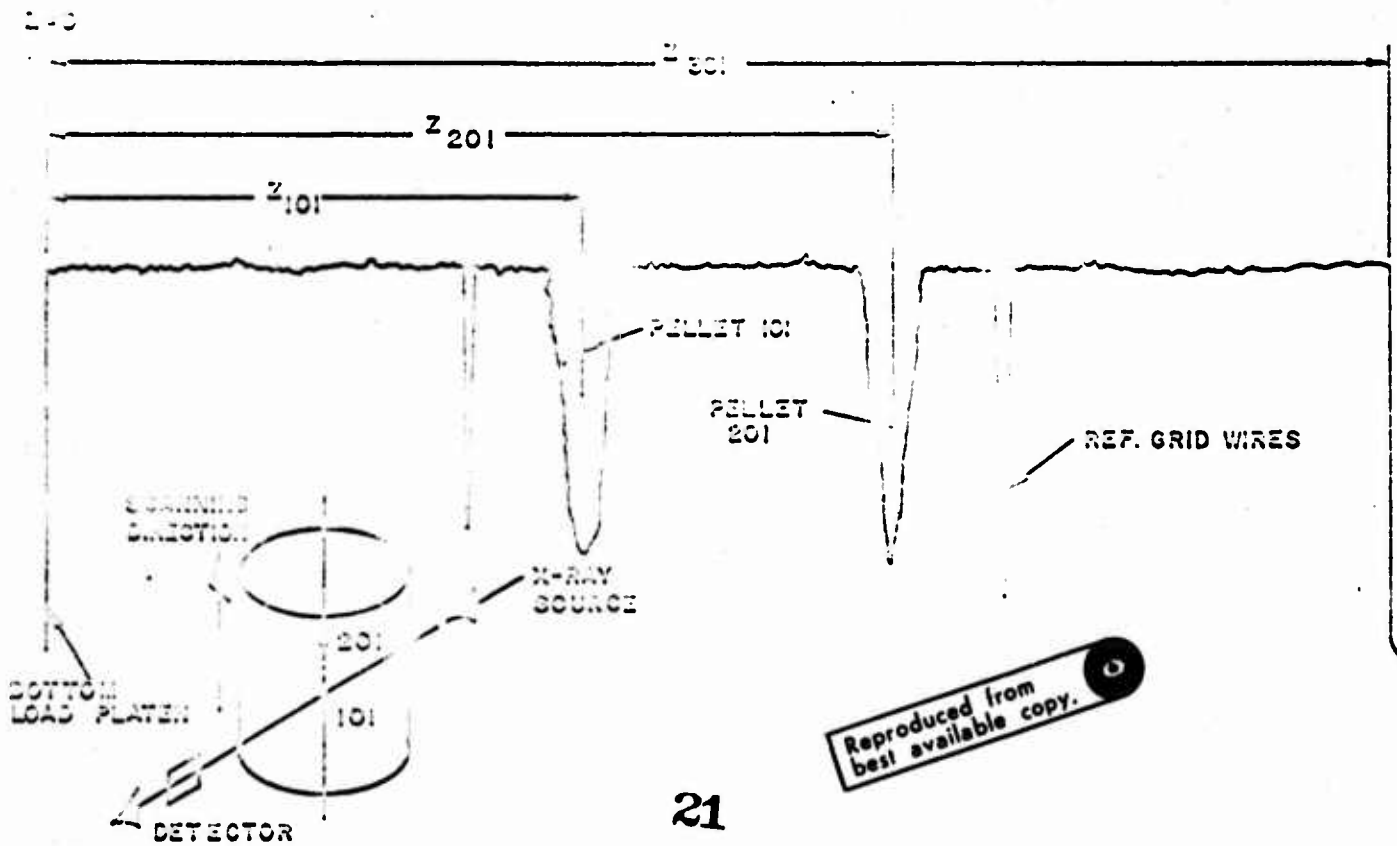
FIGURE 9   TYPICAL LONGITUDINAL TRACE
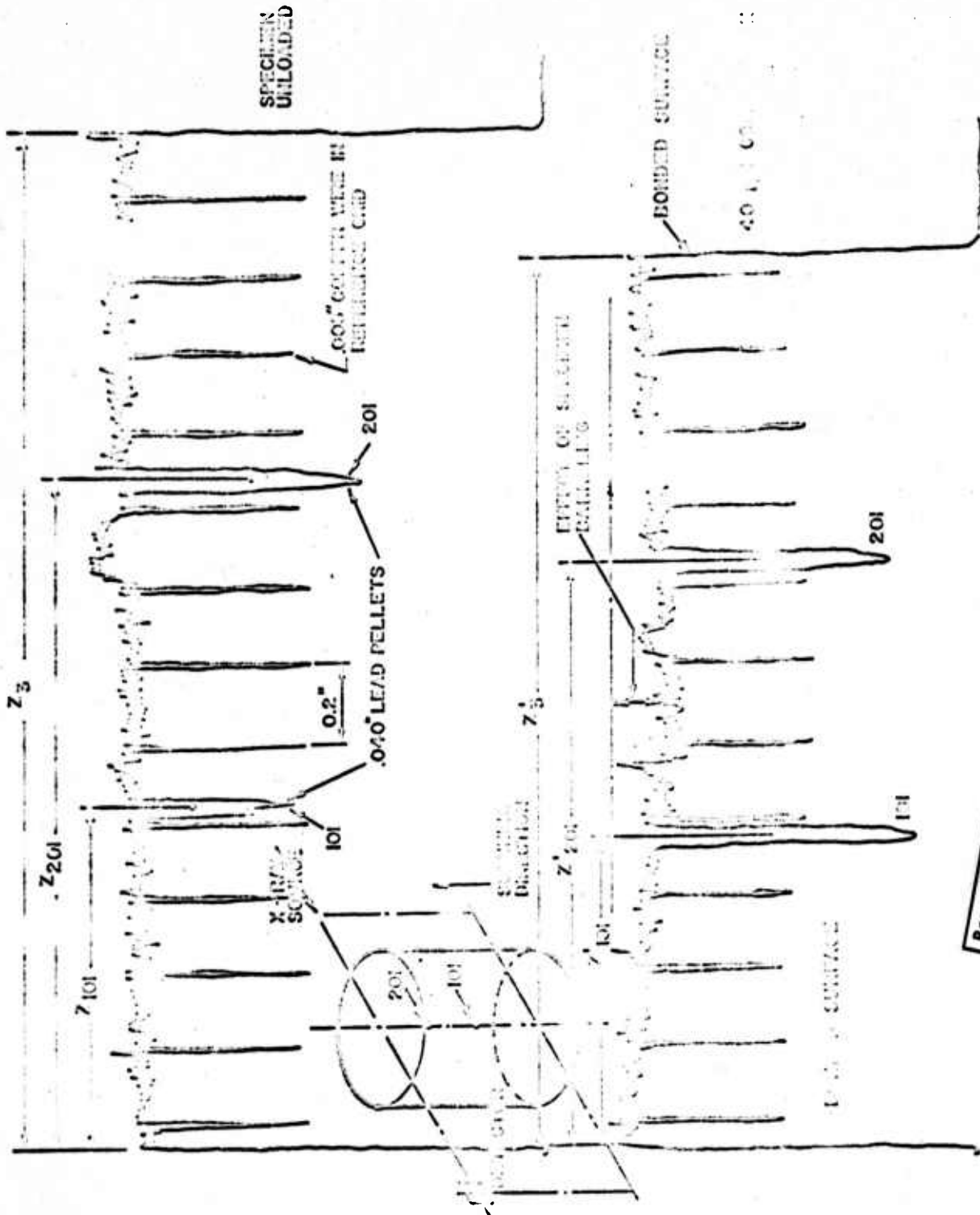
FIGURE 10   LONGITUDINAL TRACES FOR UNIAXIALLY LOADED,
FREE STANDING SOLID PROPELLANT GRAIN WITH
BONDED LOAD SURFACES
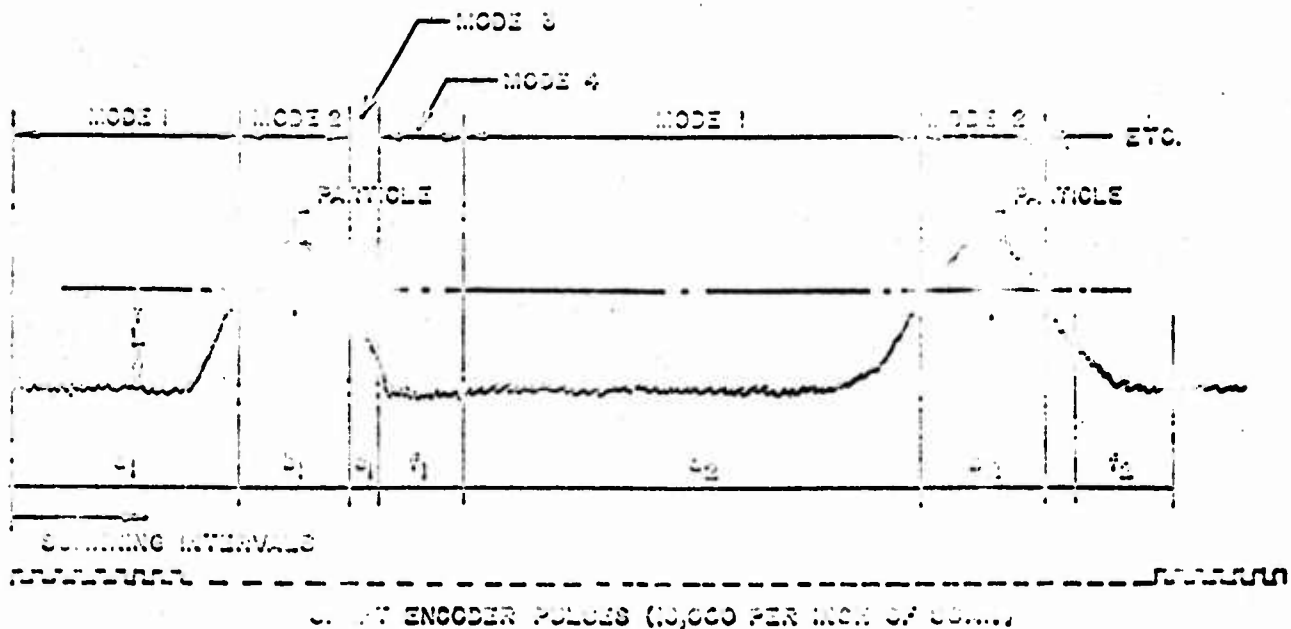
MODE 1: ALL ENCODER PULSES FED TO ACCUMULATOR.

MODE 2: HALF OF ENCODER PULSES FED TO ACCUMULATOR, HALF
TO TEMPORARY STORAGE.

MODE 3: ACCUMULATOR PRINT-OUT TRIGGERED, ALL ENCODER
PULSES FED TO TEMPORARY STORAGE (200 MILLI-
SECONDS).

MODE 4: ENCODER PULSES FED TO ACCUMULATOR; PULSES IN
TEMPORARY STORAGE TRANSFERRED TO ACCUMU-
LATOR.

FIGURE 11   OPERATION MODES OF DIGITAL
READOUT SYSTEM
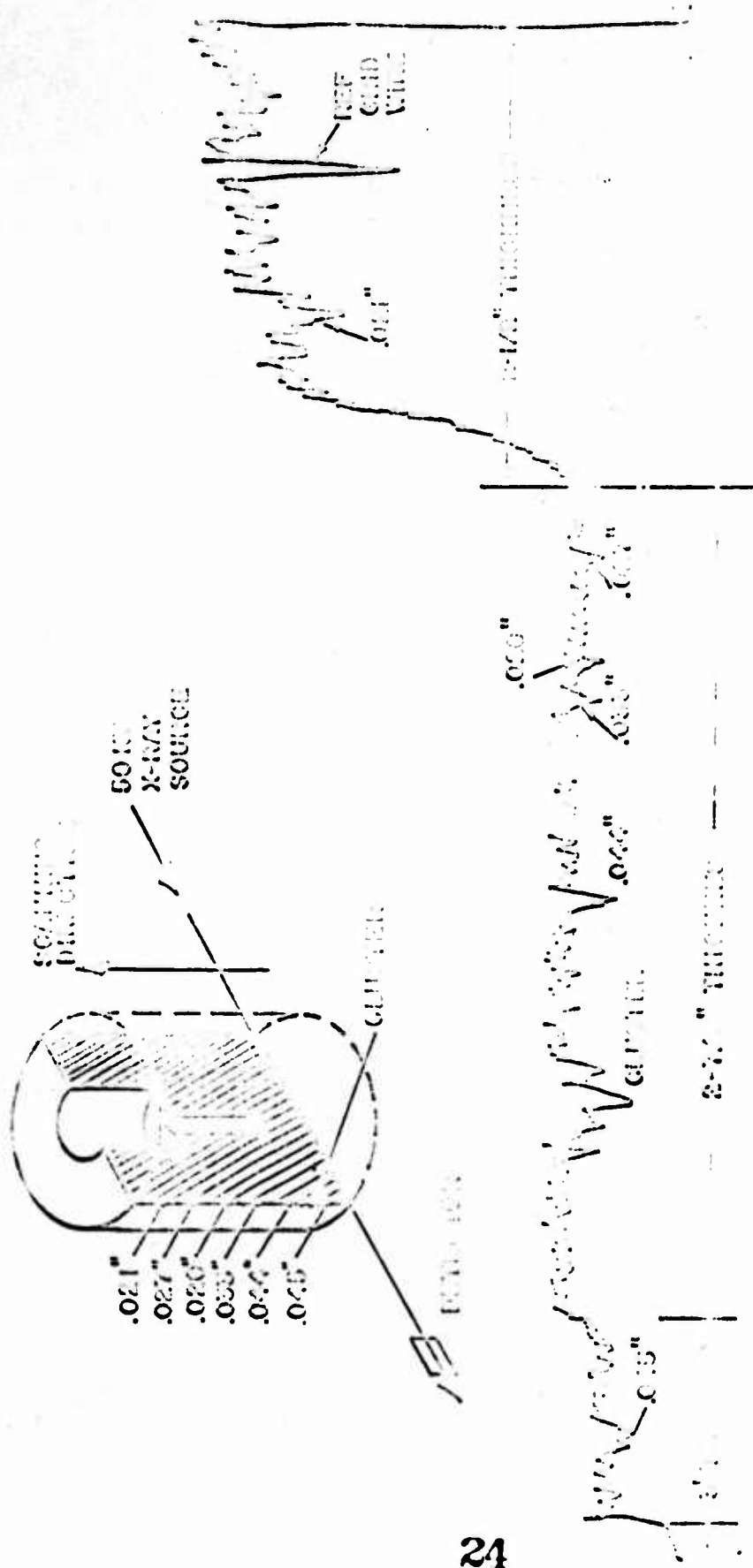
FIGURE 12 LEAD PELLET RESOLUTION -
SOLID PREPELLANT (80% SOLID)

24

FIGURE 13   GLASS PELLET RESOLUTION -
INERT SOLID PROPELLANT
(90% SOLID)
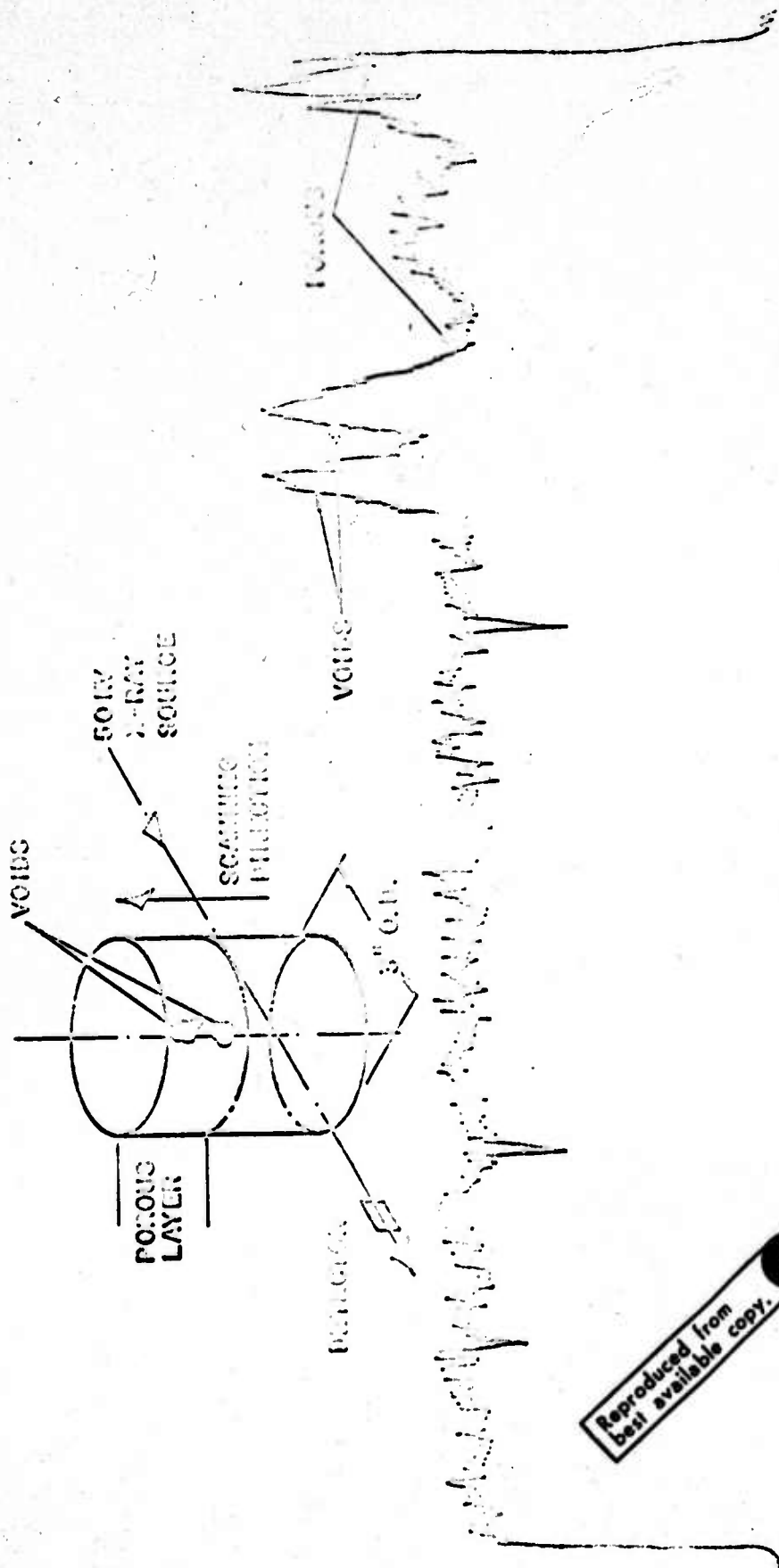
FIGURE 14 VOID POROSITY RESOLUTION - INERT SOLID PROPELLANT (80% SOLIDS)
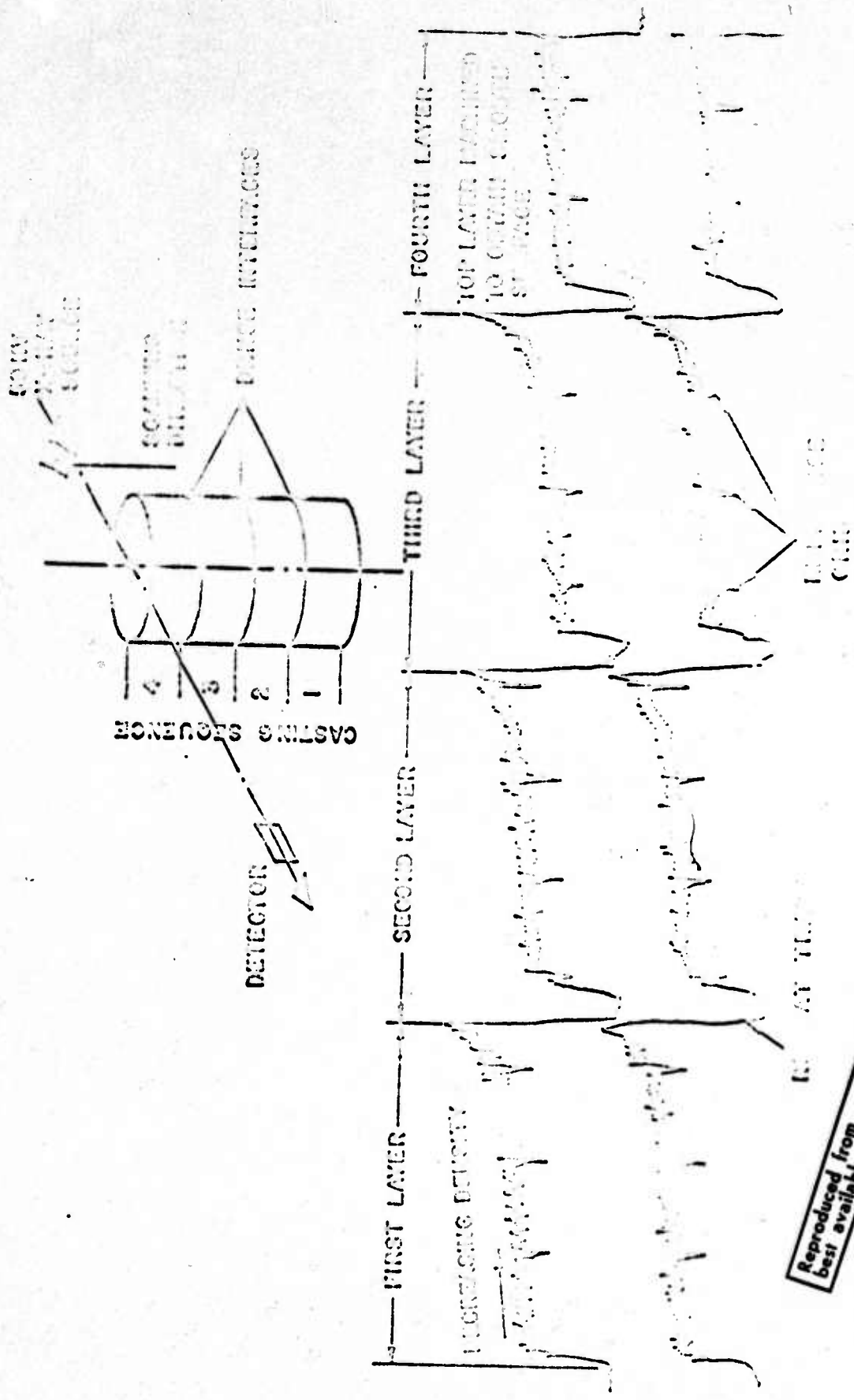
FIGURE 15   LONGITUDINAL TRACES OF SEGMENTALLY
CAST GRAIN WITH DENSE INTERFACES
(50% SOLID)

SOLID CYLINDER

RADIAL PLANE I=1

HOLLOW CYLINDER

RADIAL PLANE I=1
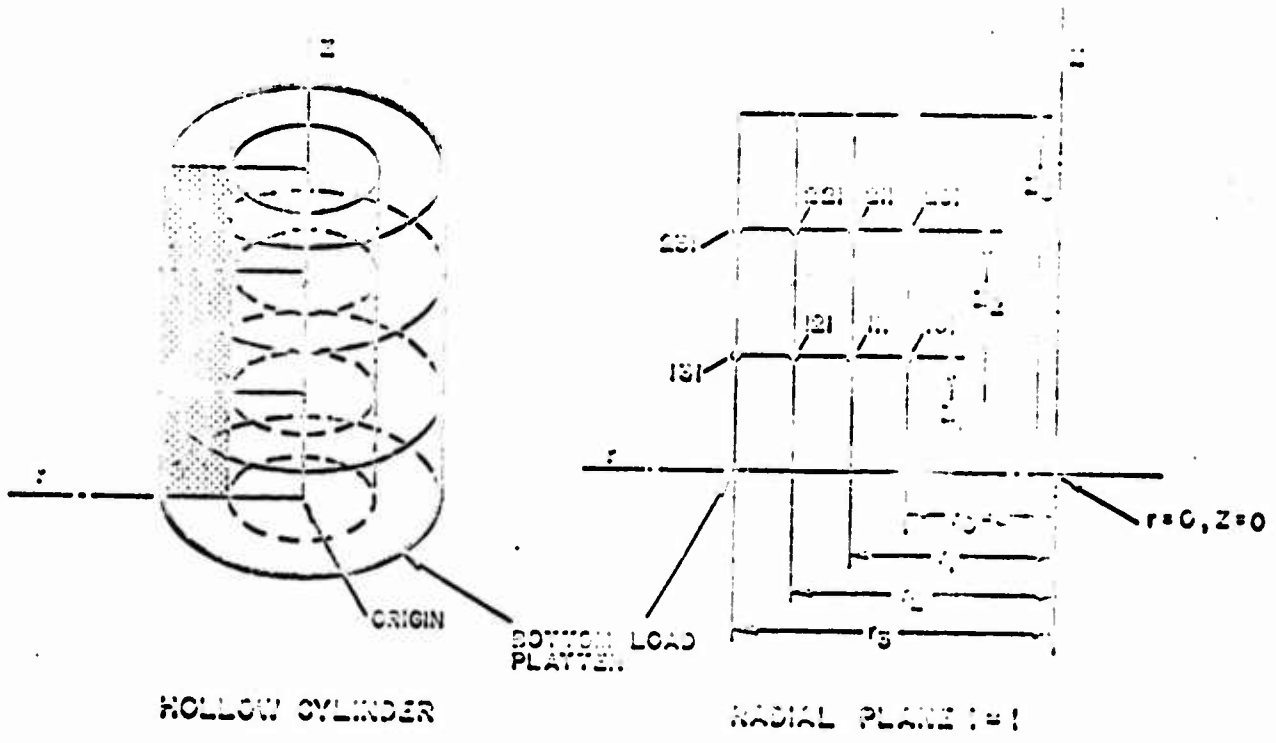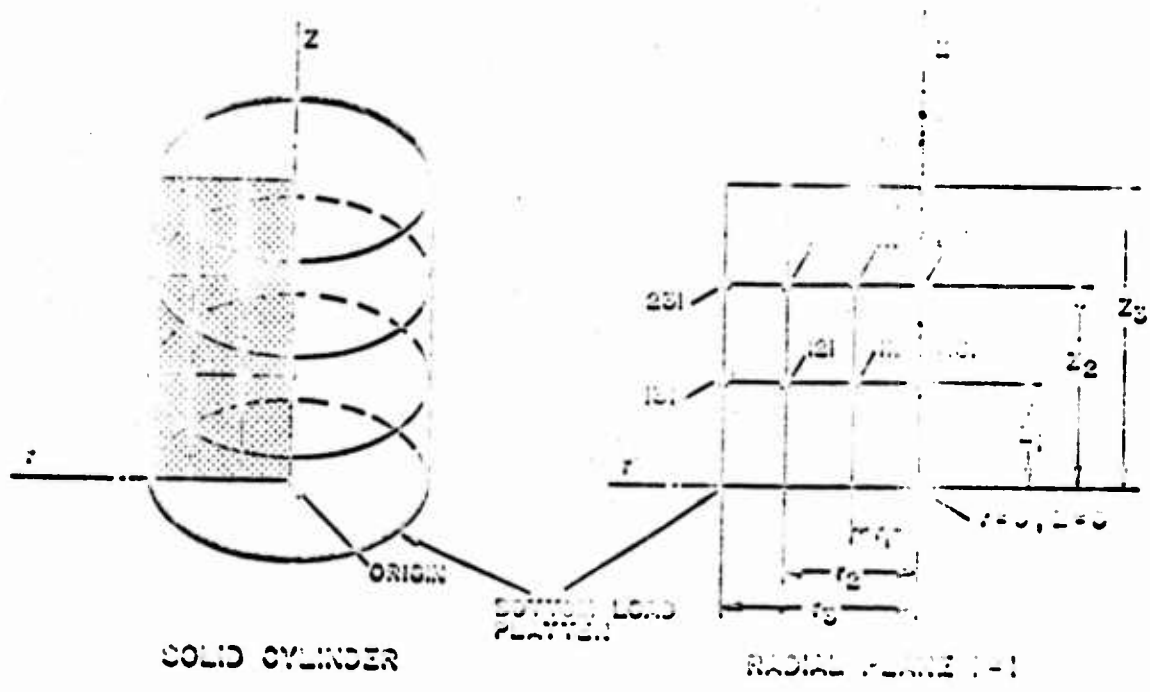
FIGURE 16   PARTICLE ARRAY AND NOTATION FOR
CYLINDRICAL GRAINS
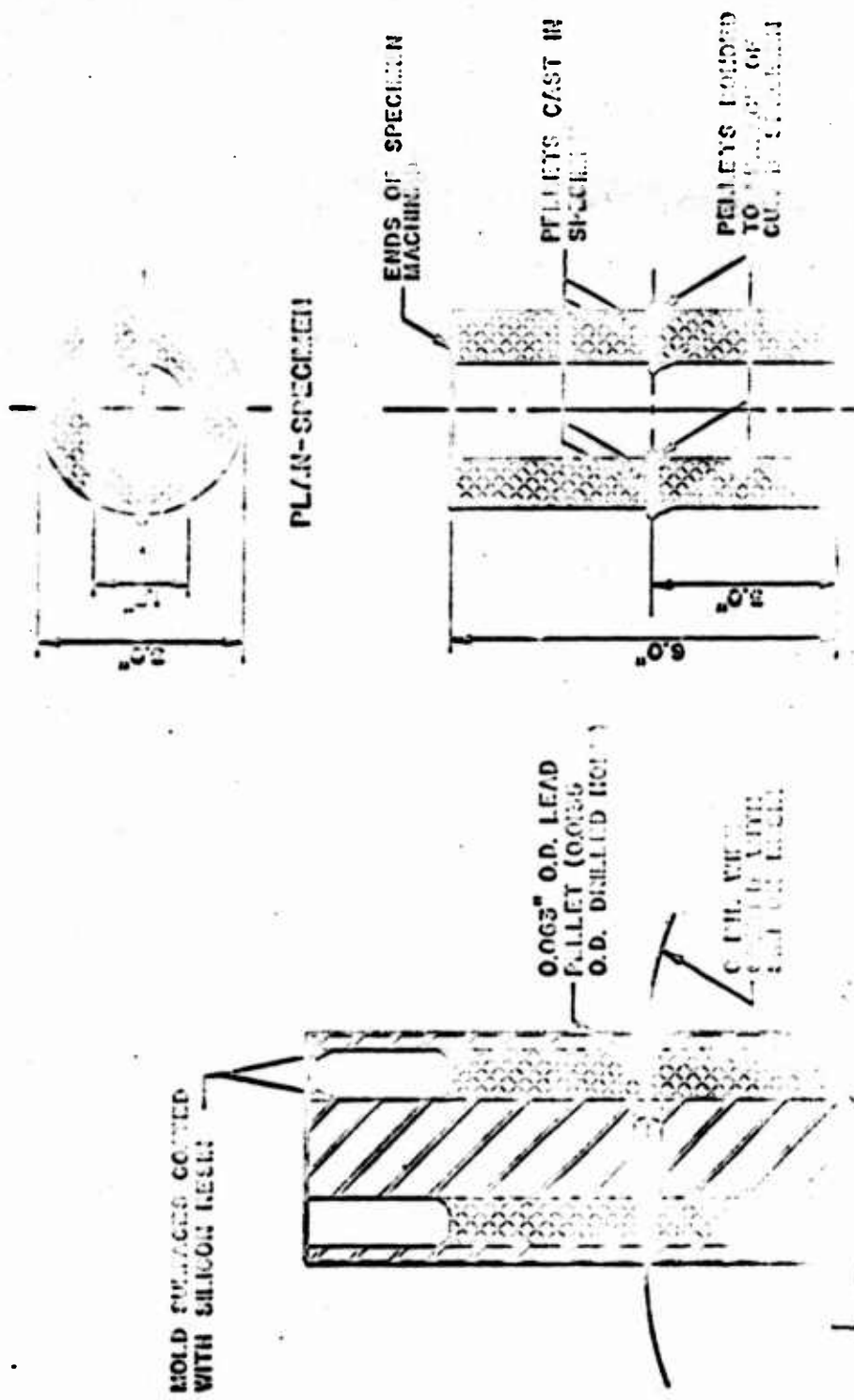
FIGURE 17 CONTINUOUS CASTING PROCEDURE FOR
PREPOSITIONED EMBEDDED PARTICLES

29

0.025"

8.38"O.D.
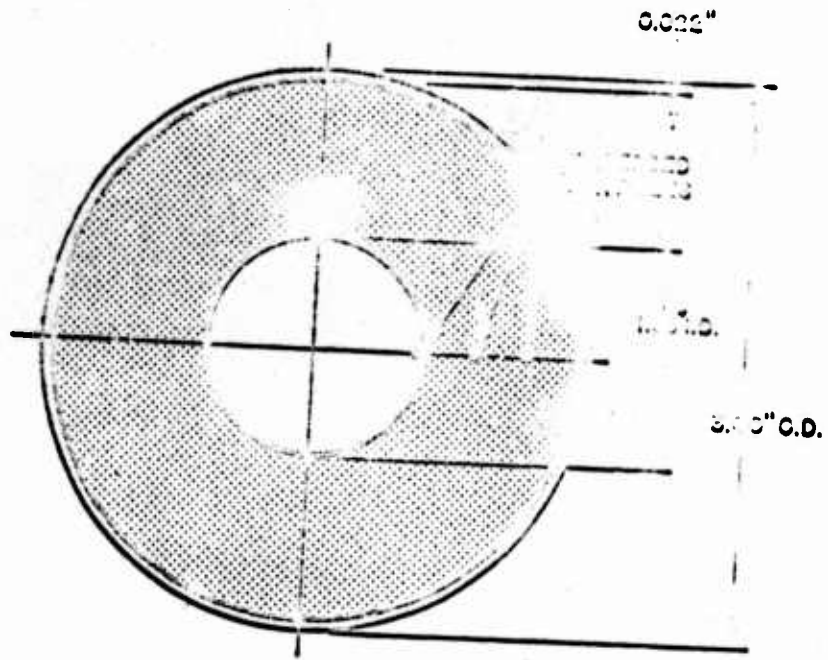
FIGURE 18   CASE-BONDED GRAIN WITH CIRCULAR CORE

0.012"

EMBEDDED
PARTICLES

2.00"

3.00"O.D.

30
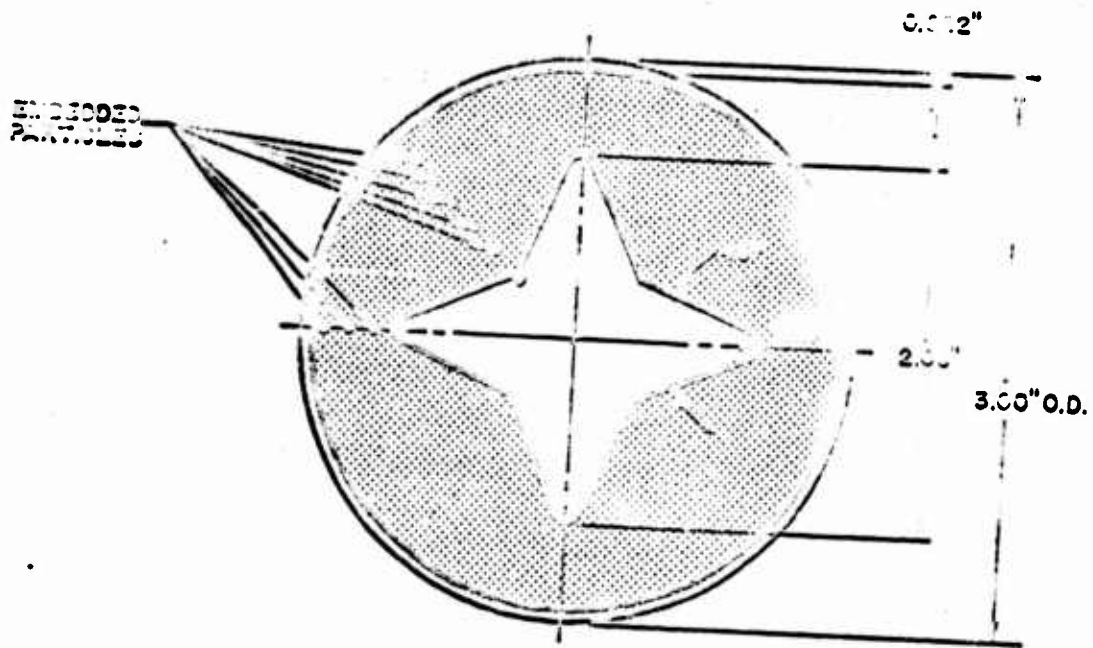
FIGURE 19   CASE-BONDED GRAIN WITH STAR-SHAPED CORE
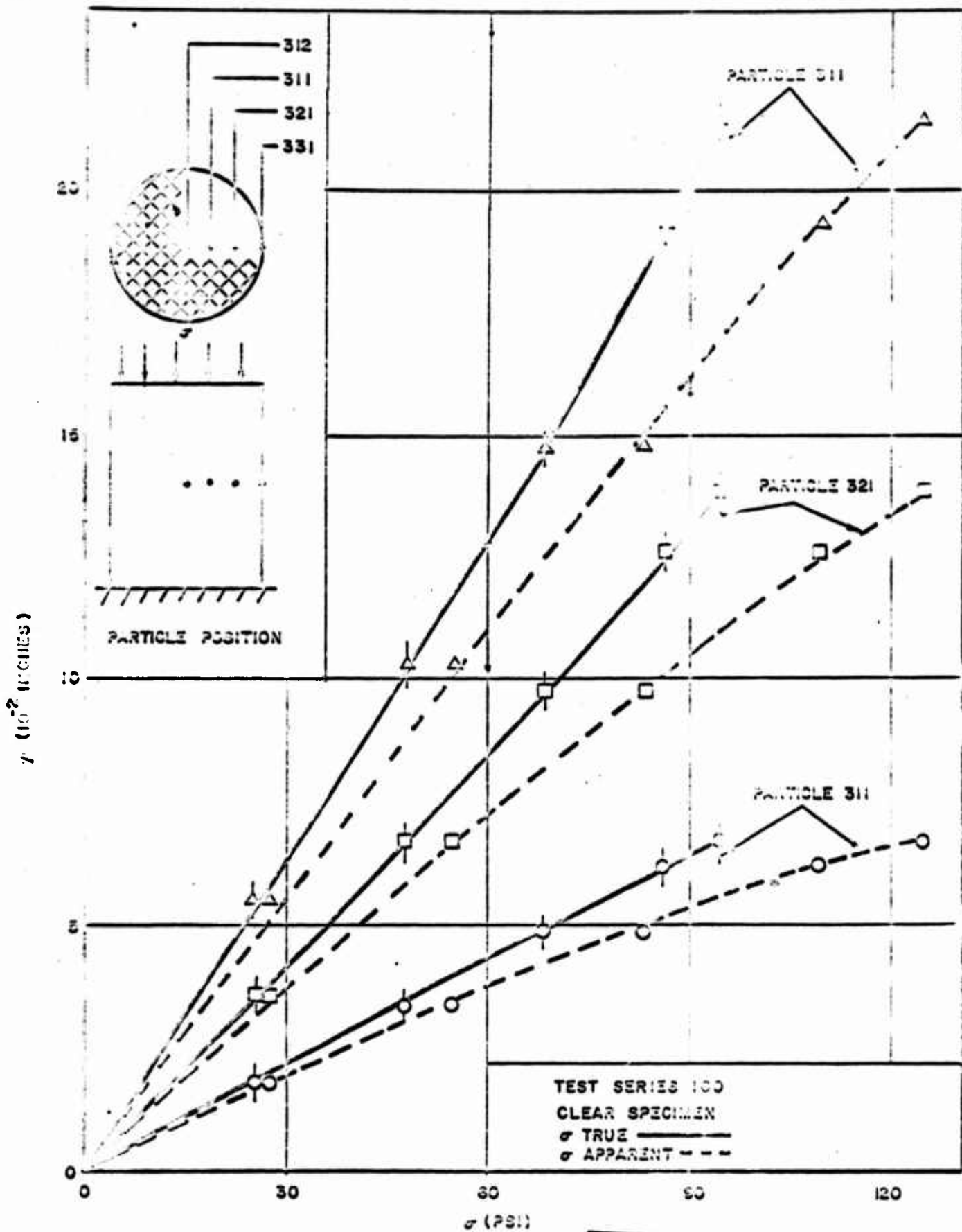
FIGURE 20   RADIAL DISPLACEMENT OF EMBEDDED
PARTICLES VERSUS AXIAL STRESS

31
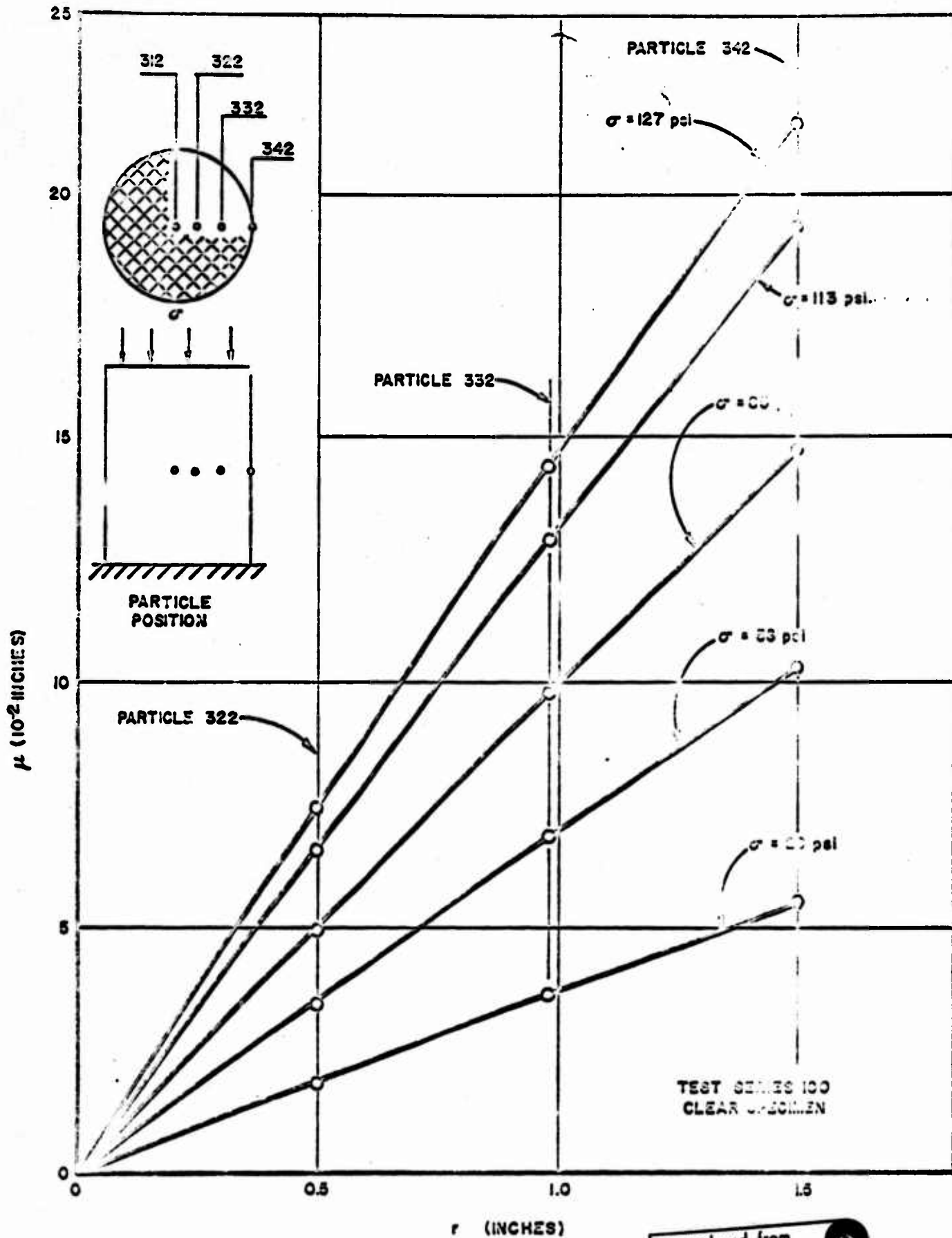
FIGURE 21   RADIAL DISPLACEMENT VERSUS INITIAL RADIAL
POSITION OF EMBEDDED PARTICLES - SPECIMEN

32
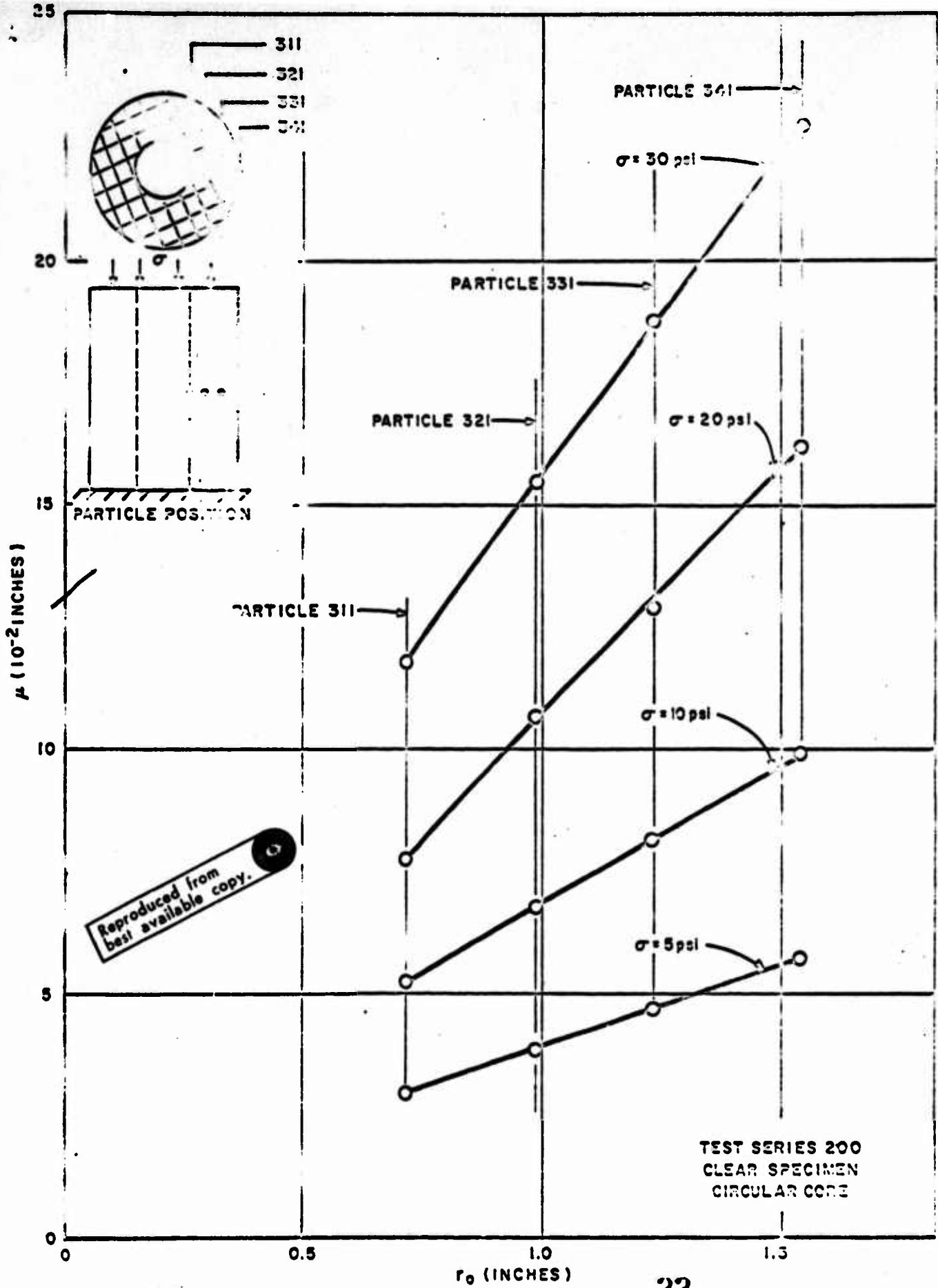
FIGURE 22   RADIAL DISPLACEMENT VERSUS INITIAL RADIAL
POSITION OF EMBEDDED PARTICLES FOR
SPECIMEN UNDER AXIAL STRESS
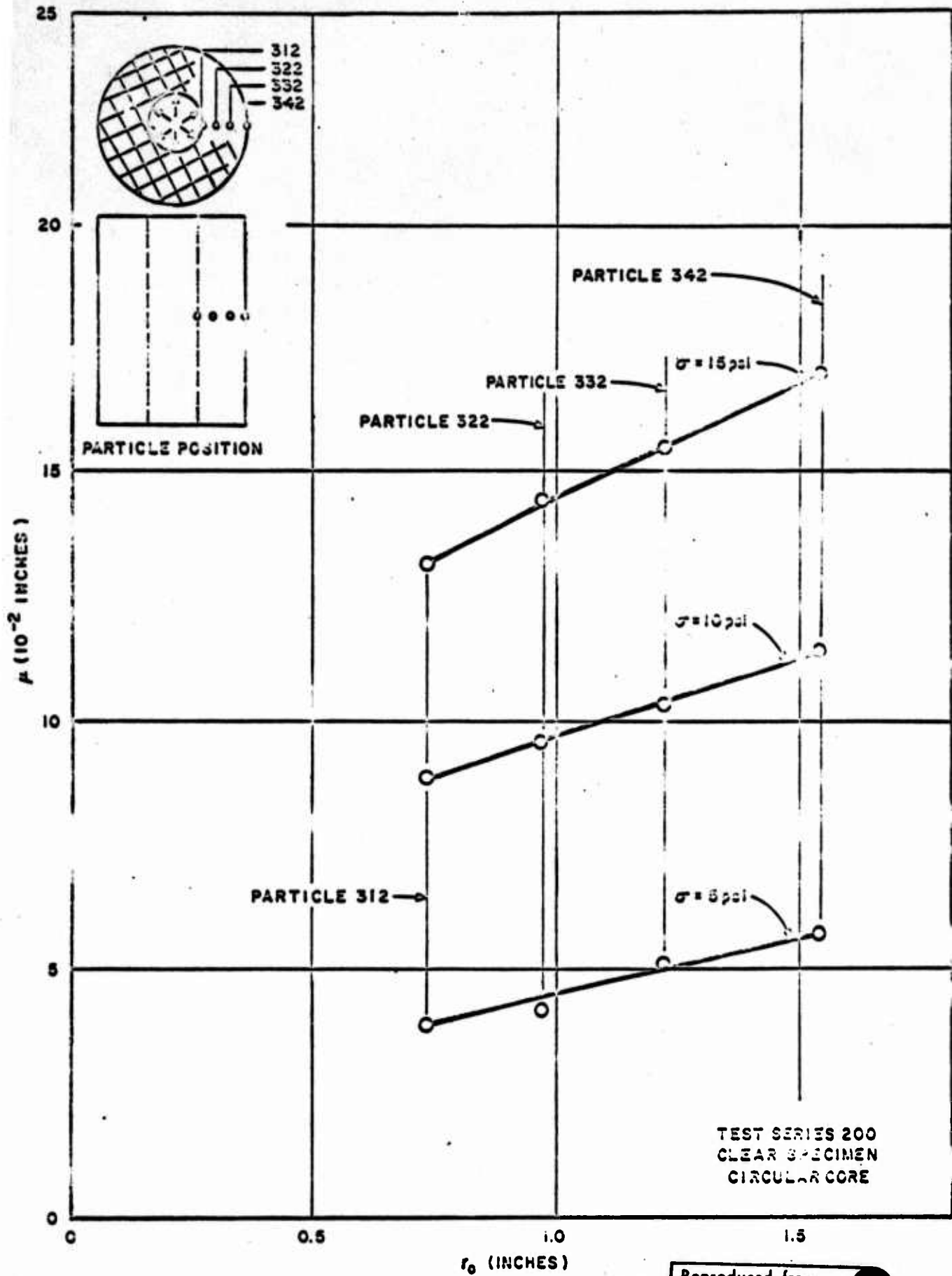
FIGURE 23   RADIAL DISPLACEMENT VERSUS INITIAL RADIAL POSITION
OF EMBEDDED PARTICLES FOR SPECIMEN UNDER
INTERNAL PRESSURIZATION

35
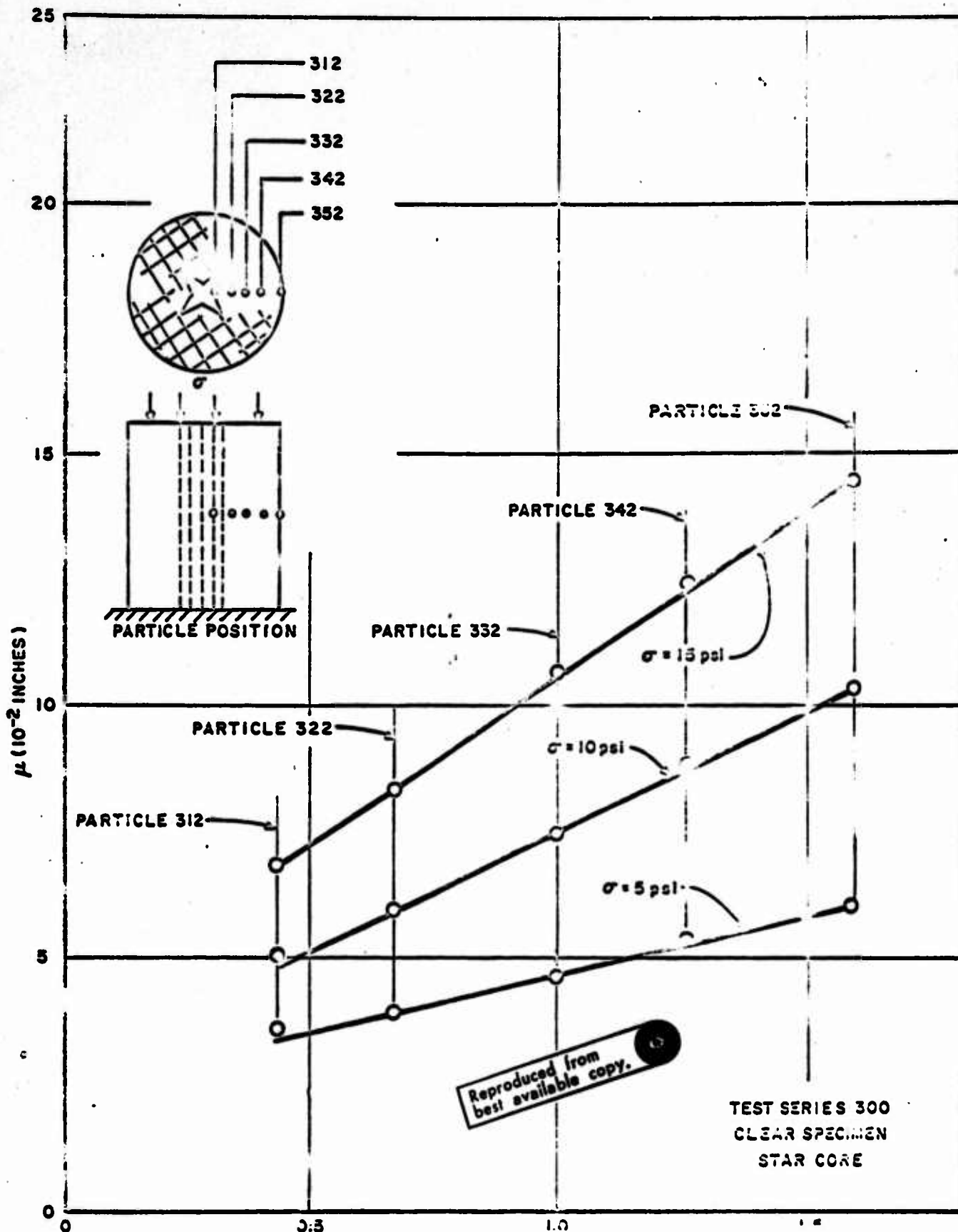
FIGURE 24   RADIAL DISPLACEMENT VERSUS INITIAL RADIAL POSITION
OF EMBEDDED PARTICLES FOR SPECIMEN UNDER AXIAL STRESS
(RADIAL PLANE 2)

36
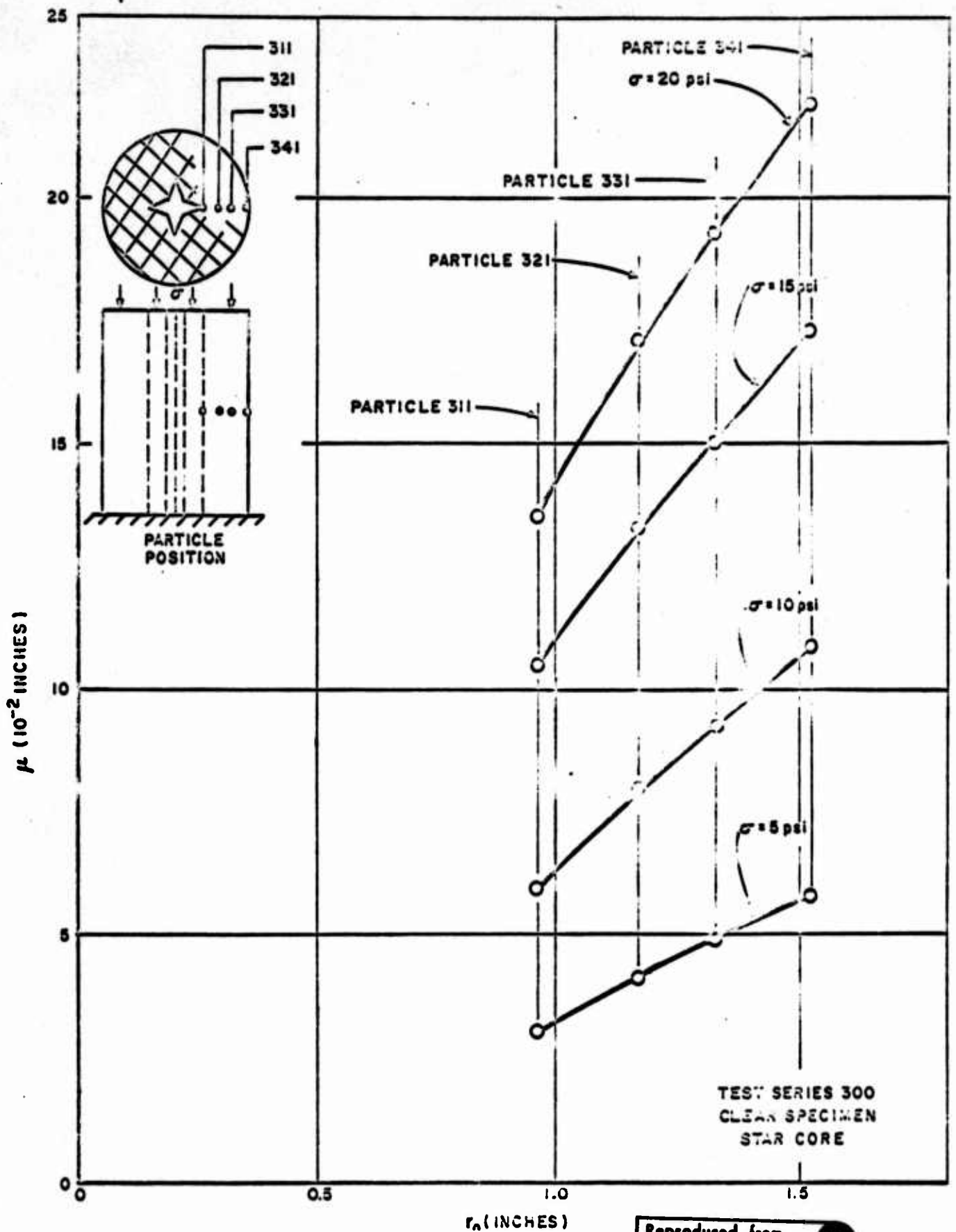
FIGURE 25 RADIAL DISPLACEMENT VERSUS RADIAL POSITION OF EMBEDDED PARTICLES FOR SPECIMEN UNDER AXIAL STRESS (RADIAL PLANE 1)

(a) Triaxial Gage

(b) Three-Gage Rosette

(c) Uniaxial Gage

FIGURE 26 CONCEPTUAL ELASTOMERIC STRAIN GAGE PROTOTYPES
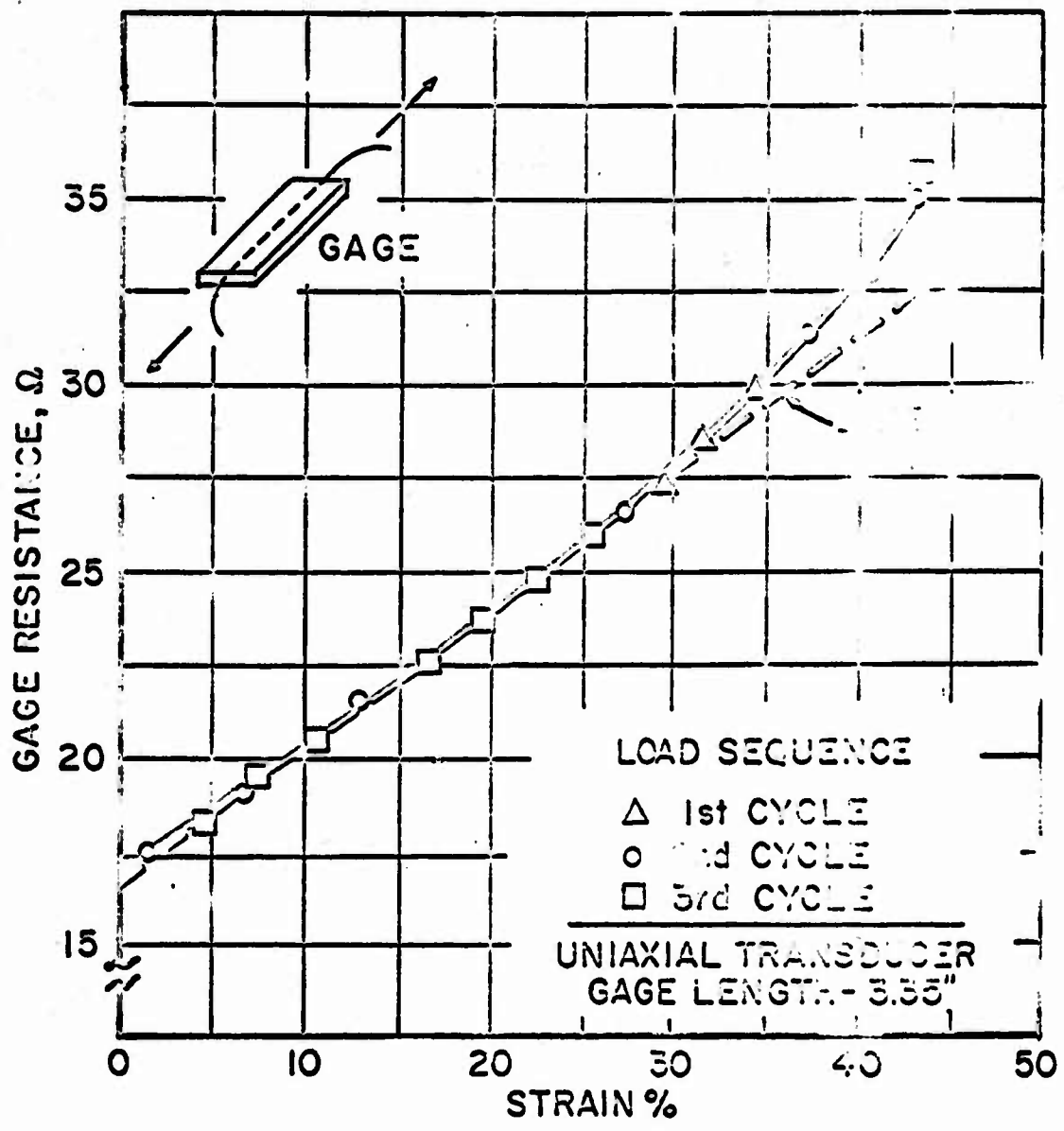
FIGURE 27   GAGE RESISTANCE VERSUS STRAIN FOR
UNIAXIAL ELASTOMERIC TRANSDUCER IN
TENSION
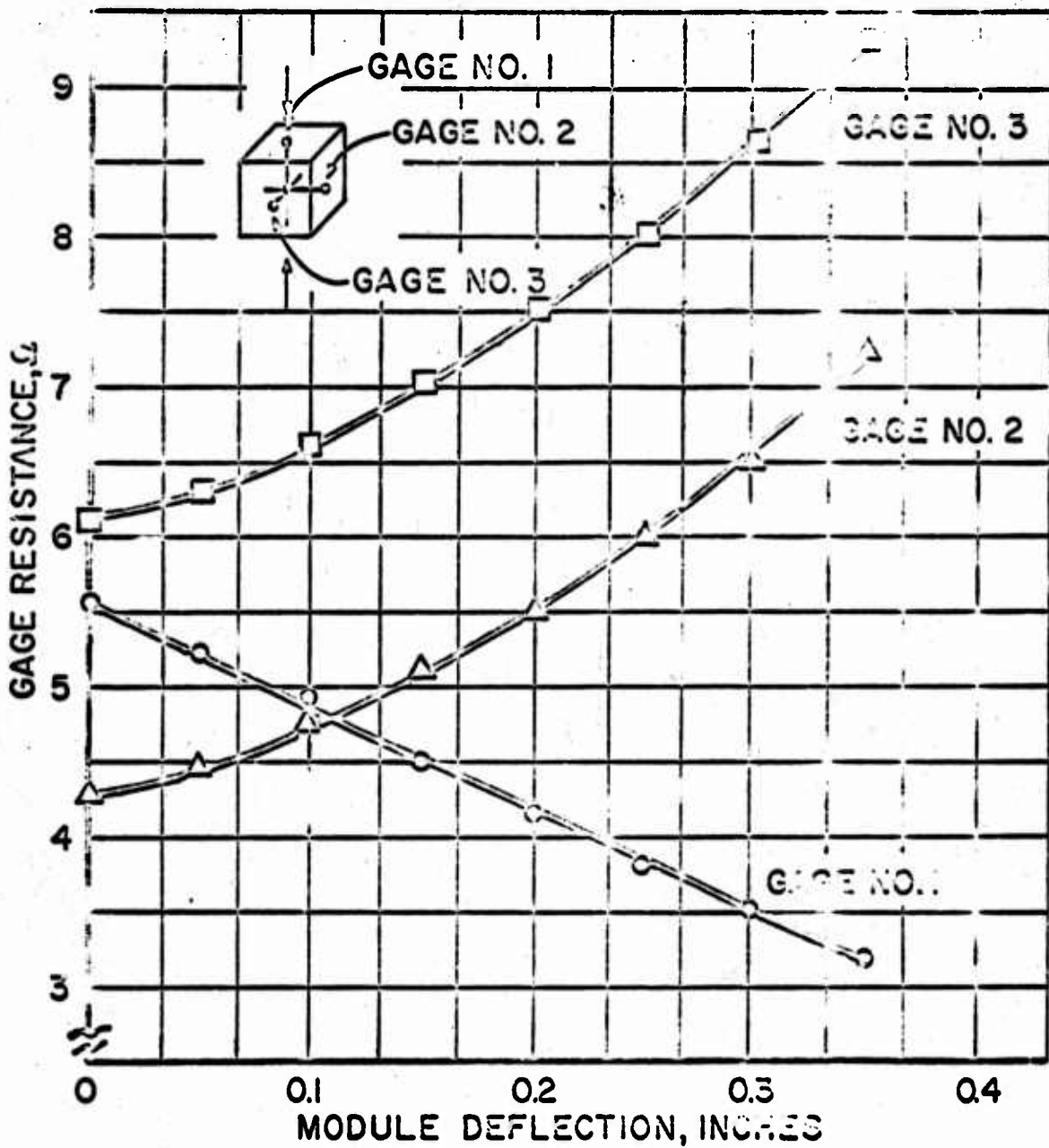
FIGURE 28   GAGE RESISTANCE VERSUS MODULE
DEFLECTION FOR TRIAXIAL TRANSDUCER

39
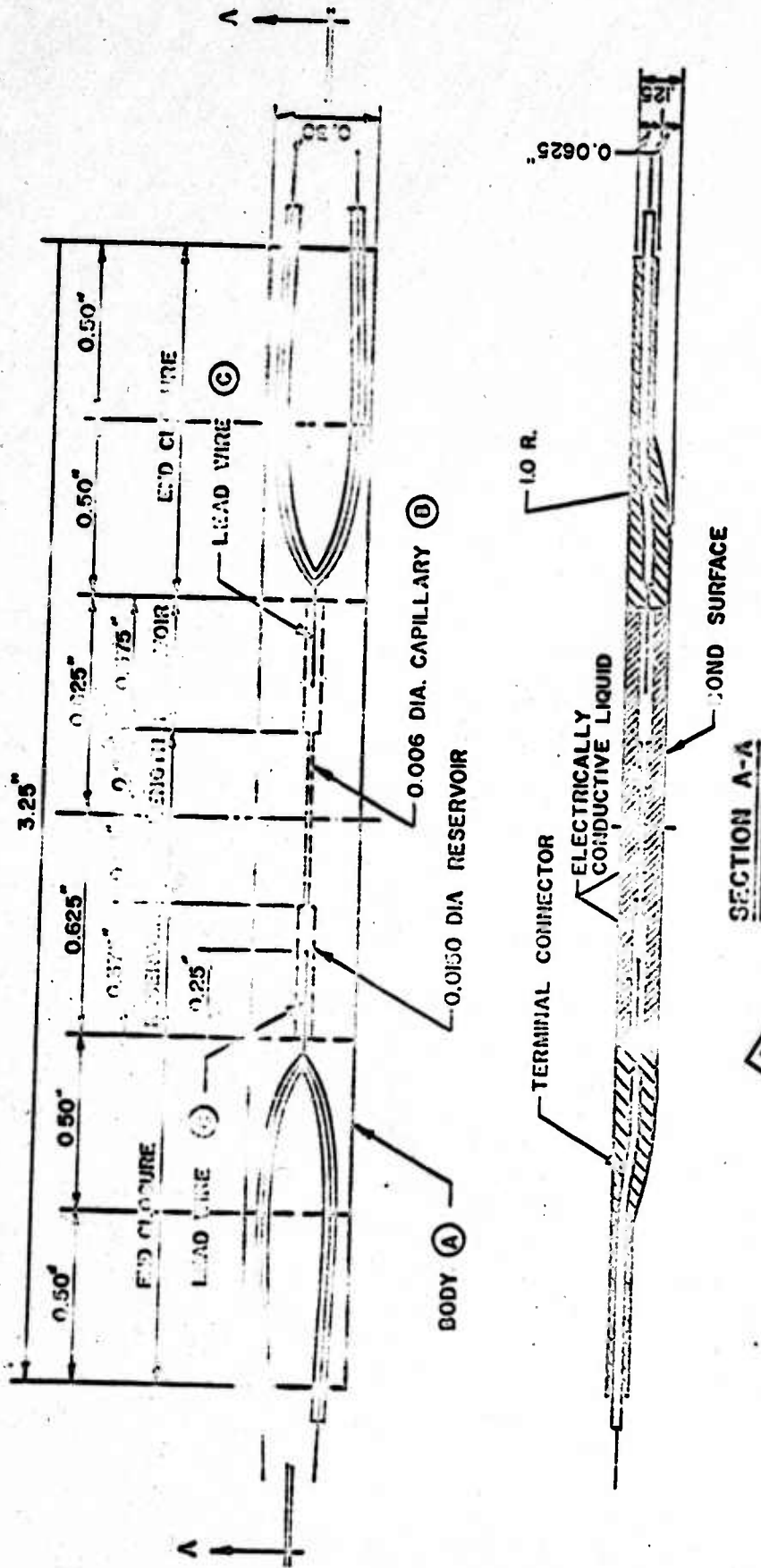
GAGE RESISTANCE: 0.30-0.60 OHMS
MATERIALS:
A. GAGE BODY — POLYURETHANE, TOLYLENE
   DI-ISOCYANATE
B. ELECTRICALLY CONDUCTING LIQUID
   MERCURY BASE ALLOY
C. TERMINAL CONNECTIONS - COPPER WIRE

FIGURE 29 ELASTOMERIC STRAIN GAGE "A",
DESIGN DRAWING

HYPODERMIC NEEDLE

STEEL WIRE 6 MIL

ALL SURFACES COATED
WITH TEFLON MOLD
RELEASE COMPOUND

HYPODERMIC NEEDLE

WIRE IS HELD TAUT BY
TENSION SPRING
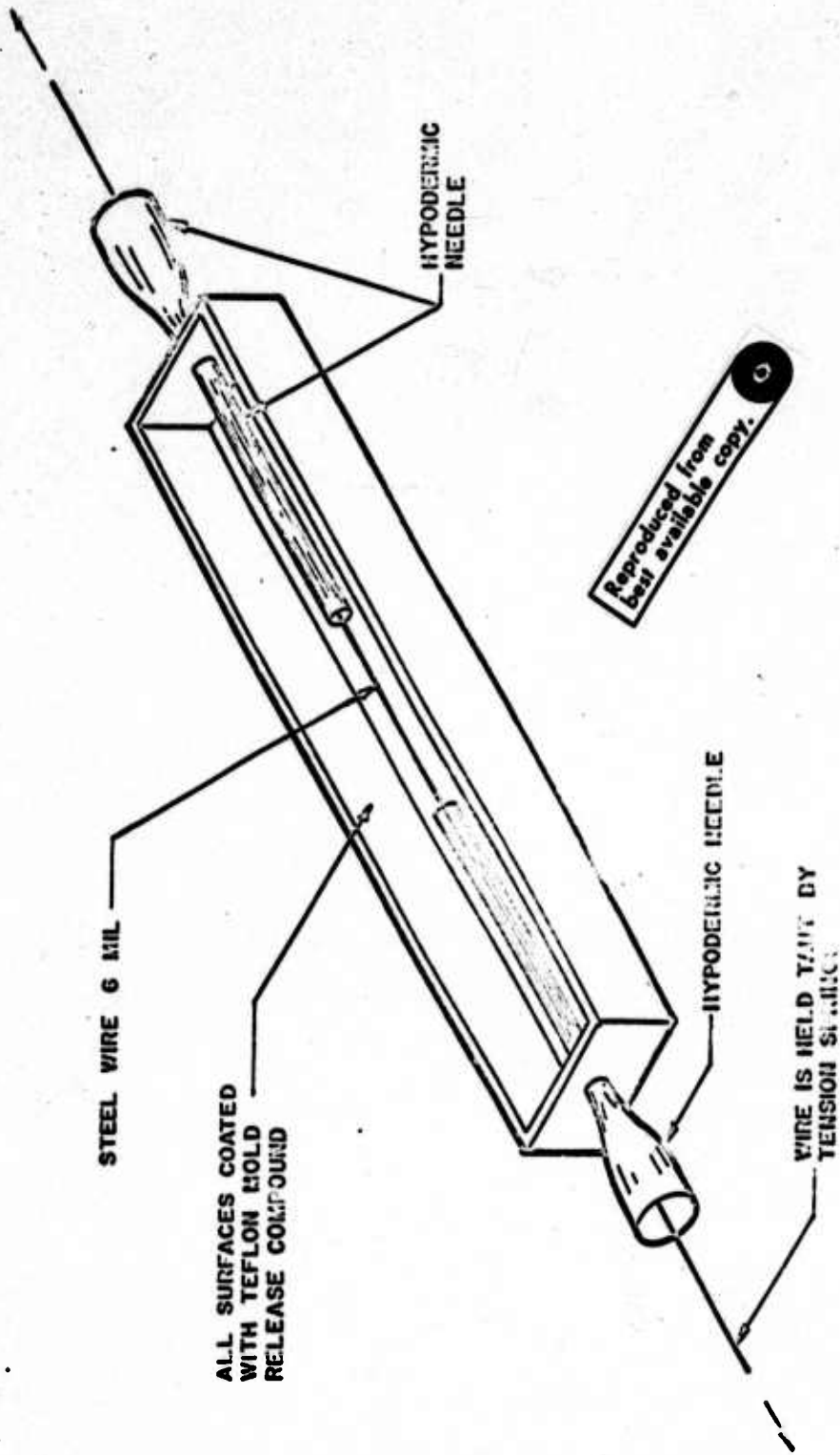
FIGURE 30 ELASTOMERIC GAGE MOLD PRIOR TO CASTING
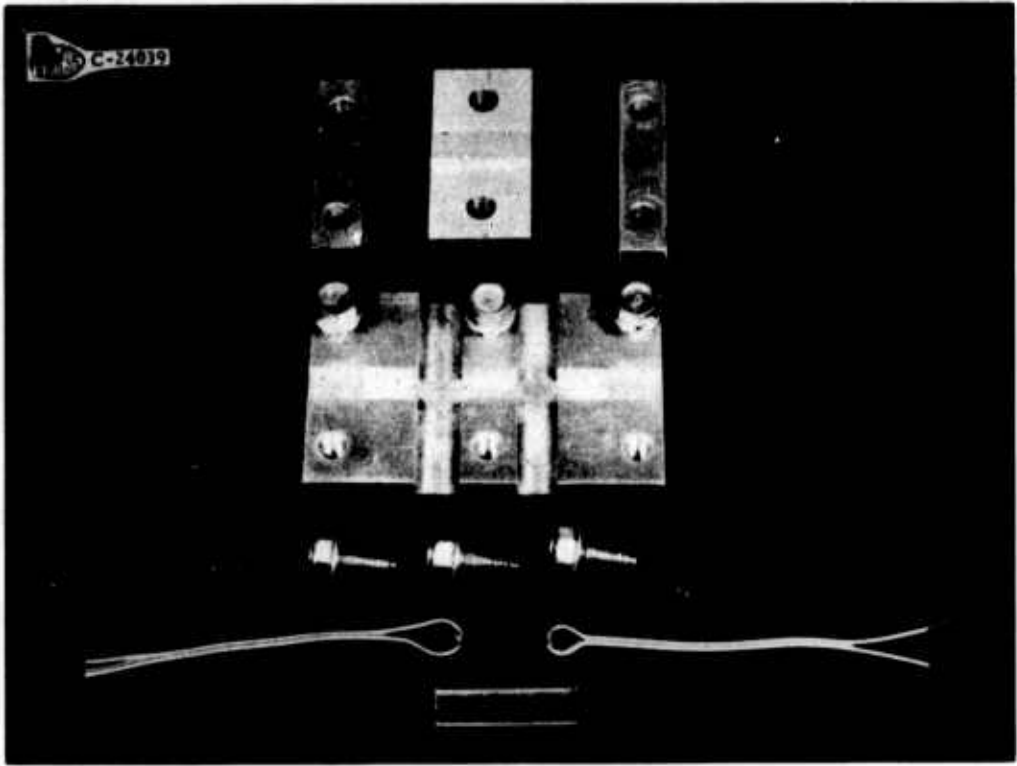
FIGURE 31   TRANSDUCER ASSEMBLING MOLD FIXTURE
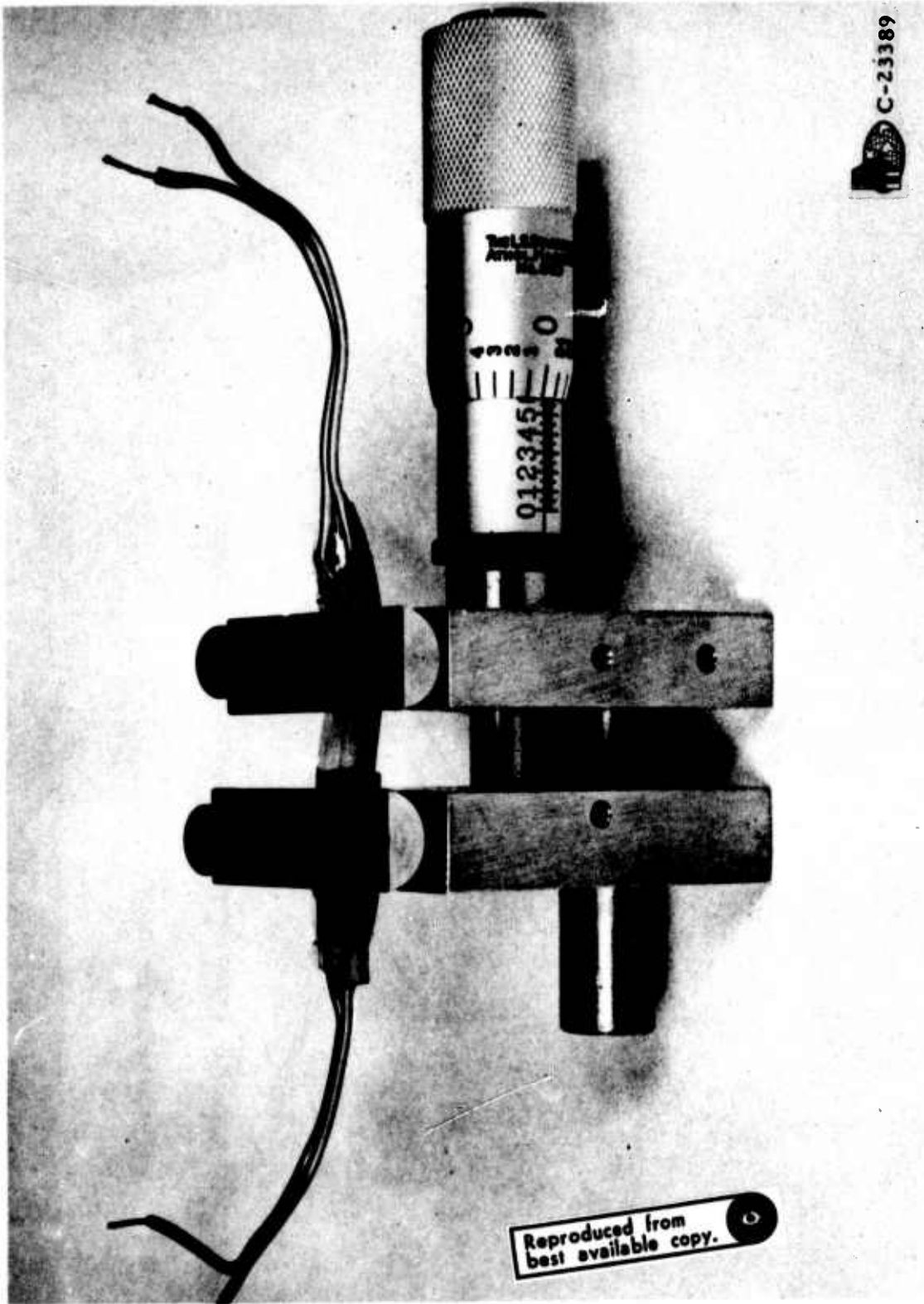
FIGURE 32   ELASTOMERIC GAGE CALIBRATION EXTENSOMETER

43
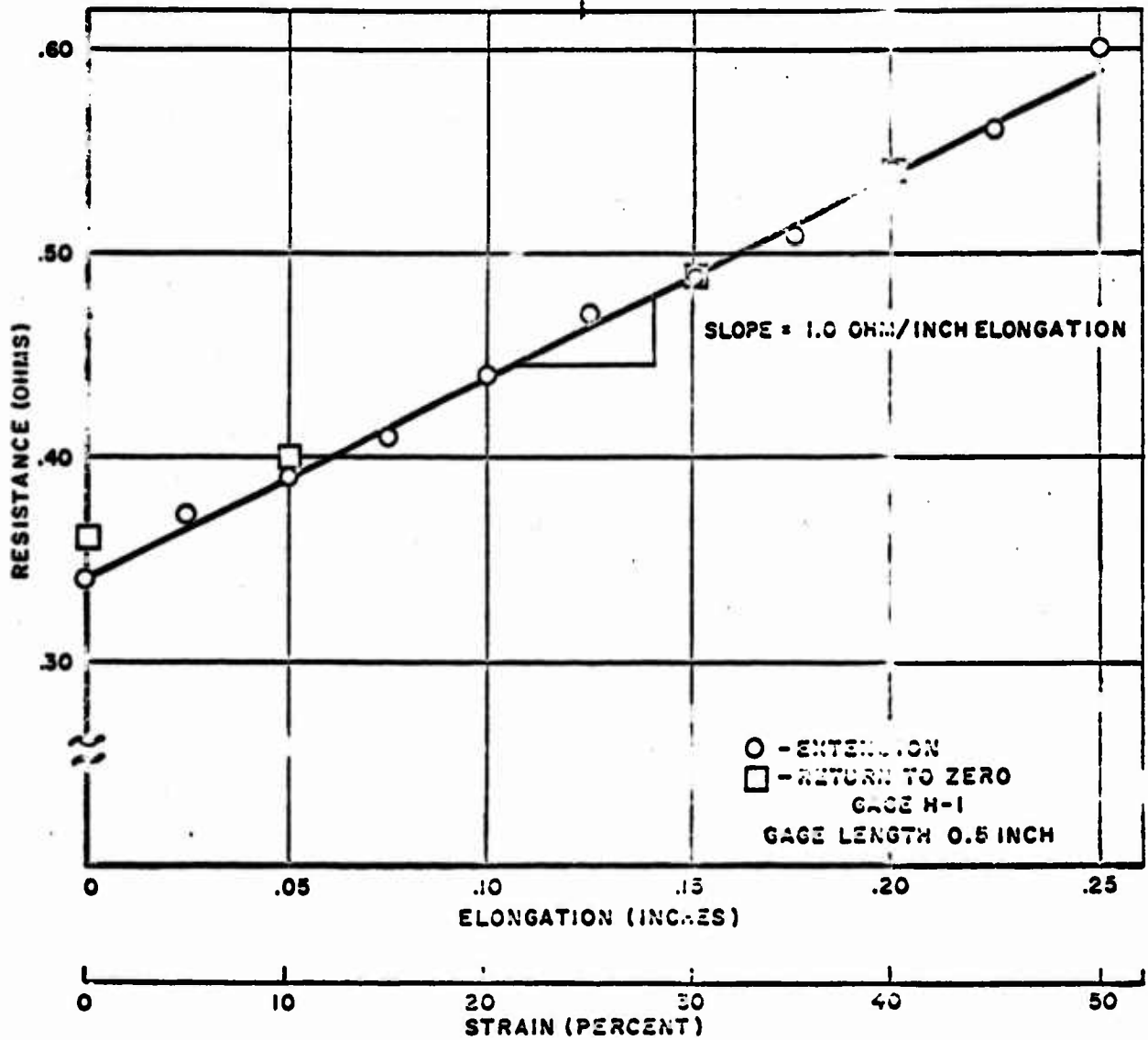
FIGURE 33   TYPICAL RESISTANCE VERSUS
GAGE ELONGATION PLOT

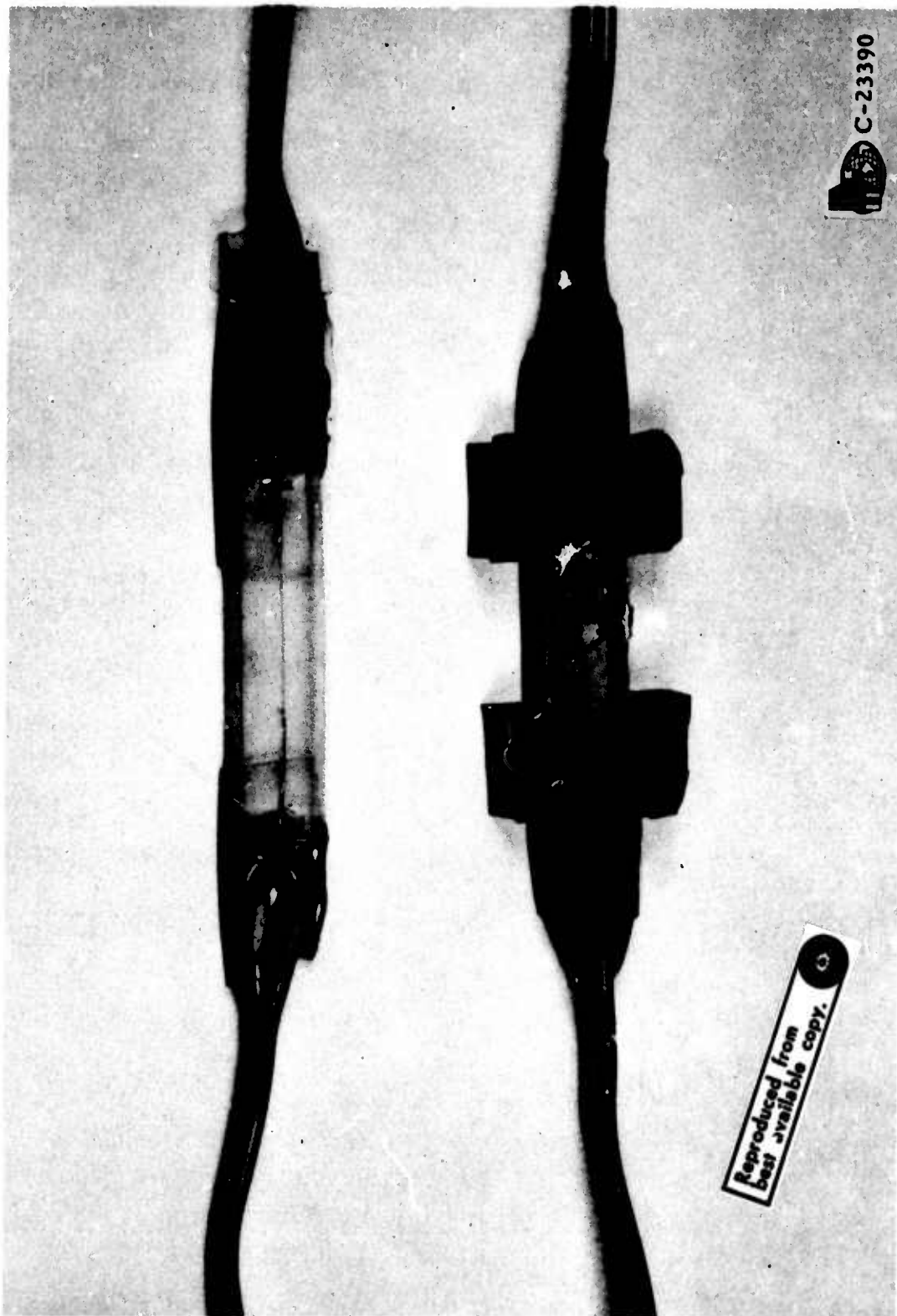44
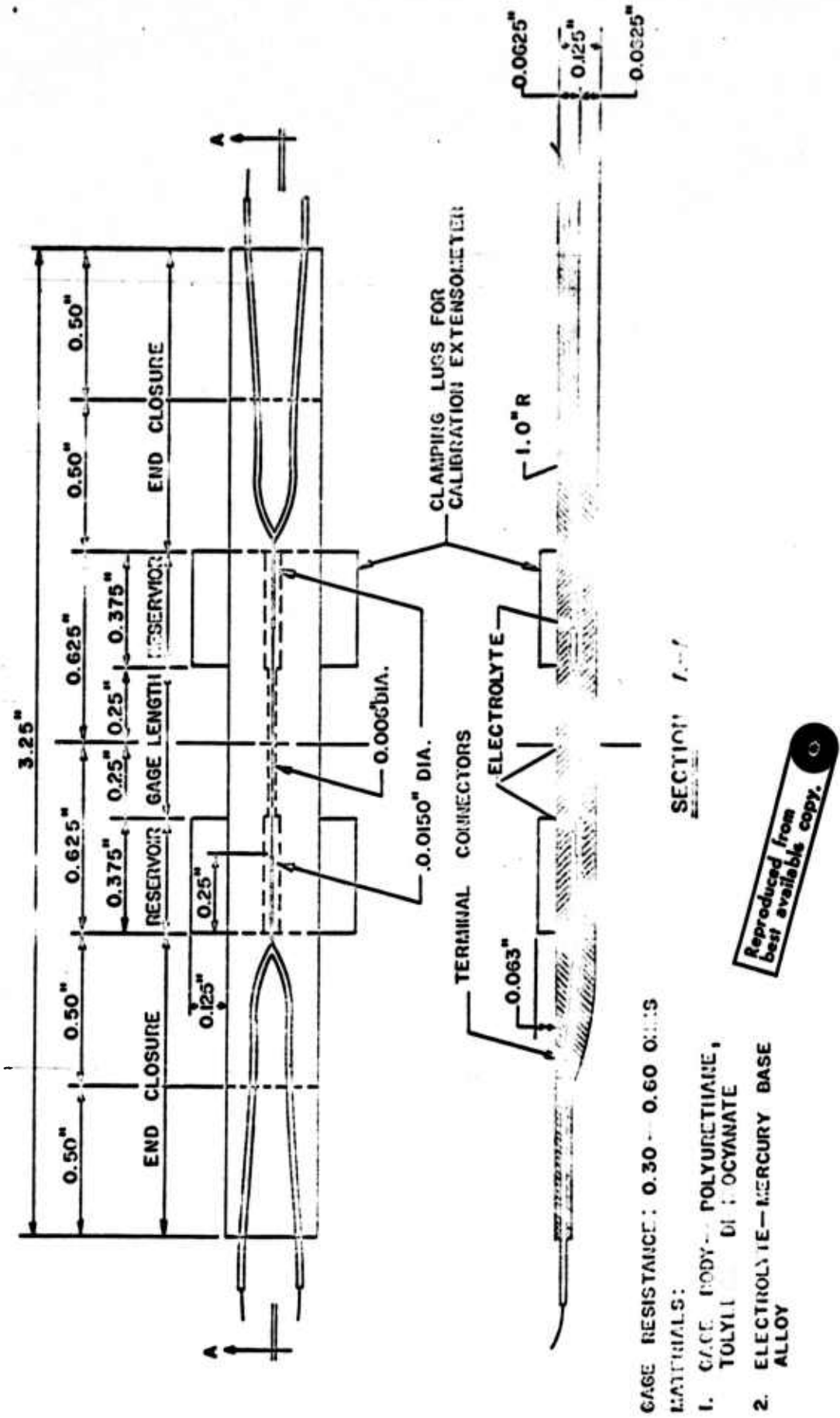
FIGURE 34 ELASTOMERIC STRAIN GAGE "II",
DESIGN DRAWING

45

FIGURE 35   STRAIN TRANSDUCER PROTOTYPES:
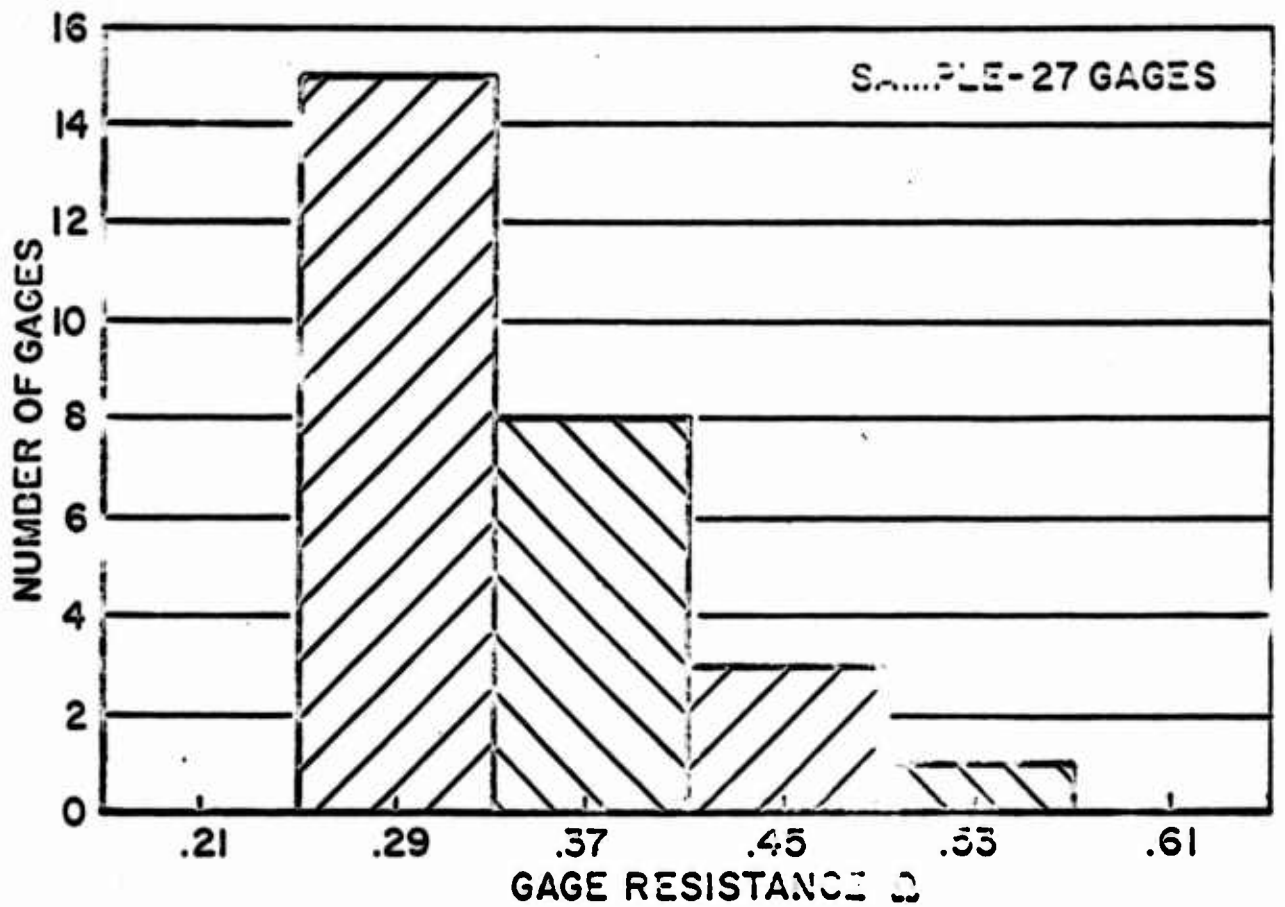ORIGINAL (UPPER) AND MODIFIED (LOWER) DESIGNS

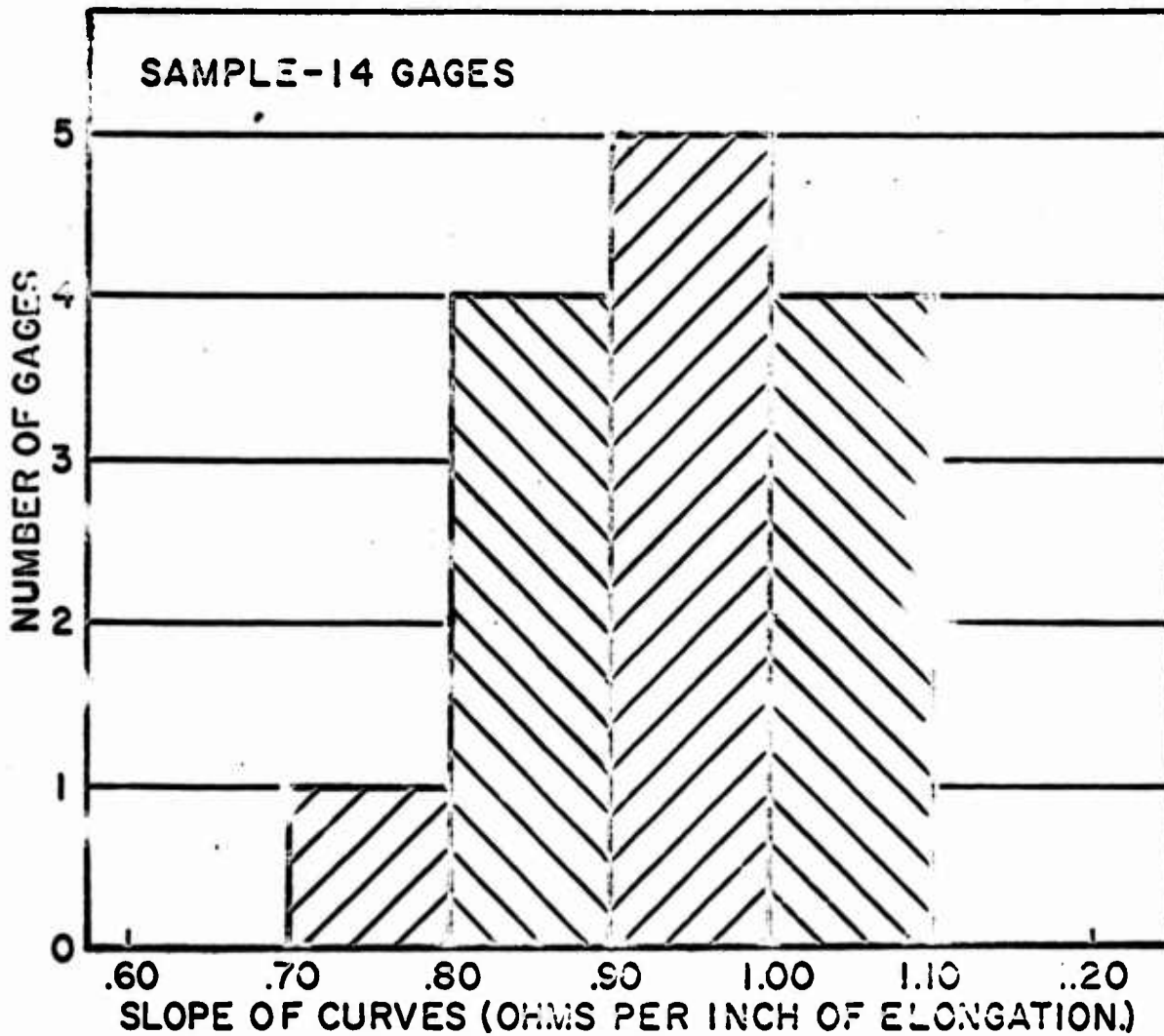FIGURE 36   FREQUENCY DISTRIBUTION OF GAGE
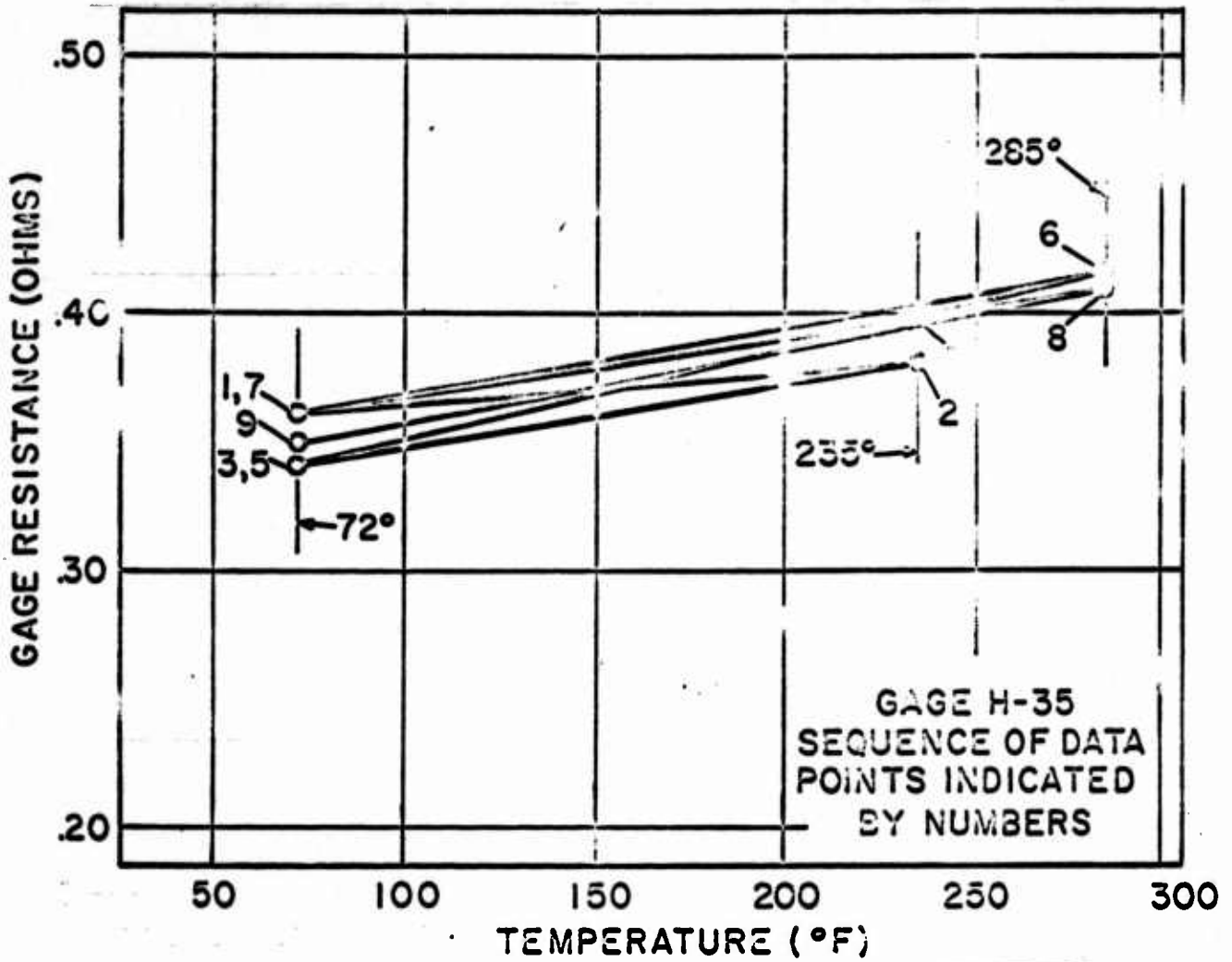RESISTANCE (0.5 INCH GAGE LENGTH)

FIGURE 37   PREQUENCY DISTRIBUTION OF SLOPES FOR
RESISTANCE VERSUS GAGE ELONGATION CURVES

48

FIGURE 38   TYPICAL PLOT OF GAGE RESISTANCE VERSUS
TEMPERATURE (FOUR CYCLES)